PhD Dissertation

무인잠수정의 최적 경로 설계 및 추적제어

Design of Optimal Trajectories and Tracking Controller for Unmanned Underwater Vehicles

Supervisor: Professor Hyeung-Sik Choi

July 2013

Graduate School of Korea Maritime University
Department of Mechanical Engineering

Mai Ba Loc

PhD Dissertation

무인잠수정의 최적 경로 설계 및 추적제어

Design of Optimal Trajectories and Tracking Controller for Unmanned Underwater Vehicles

Supervisor

Prof. Hyeung-Sik Choi

by

Mai Ba Loc

A dissertation submitted in partial fulfillment

of the requirements for the degree of

Doctor of Philosophy

at the

Department of Mechanical Engineering

Graduate School of Korea Maritime University

July 2013

본 논문을 마이바록의 공학박사 학위논문으로 인준함.

위원장: 공학박사 유삼상 (인)

위 원: 공학박사 최형식 (인)

위 원: 공학박사 황광일 (인)

위 원: 공학박사 김준영 (인)

위 원: 공학박사 김정창 (인)

2013 년 07 월 24 일

한국해양대학교 대학원

Acknowledgement

I would like to express my deep gratitude to my supervisor Professor Hyeung-Sik Choi for continuously helping and supporting me during the PhD course in Mechanical Engineering. His guidance, encouragement and patience have helped me complete my study and research.

I am grateful to Professors Sam-Sang You, Joon-Young Kim, Kwang-Il Hwang, and Jeong-Chang Kim for their advice and their words of encouragement to complete this dissertation.

I would like to also thank my lab members at the Intelligent Robot and Automation Lab – KIAL. They have helped me with a countless number of things, both academic and non-academic, during my time at Korea Maritime University - KMU. Sometimes, their words of concern and jokes warmed my heart while I was away from my homeland. We have had a lot of unforgettable memories. Thank you so much!

And lastly, but by no means least, I would like to thank my parents for their confidence and constant support. They always look forward to my calls every Sunday night to tell me stories of our family, and to give words of encouragement to me.

Mai Ba Loc

KMU, Busan, South Korea

Design of Optimal Trajectories and Tracking Controller for Unmanned Underwater Vehicles

Mai Ba Loc

Department of Mechanical Engineering
Graduate School of Korea Maritime University

Abstract

This dissertation presents the design of optimal trajectories and tracking controller for the translational motion of an unmanned underwater vehicle (UUV). The dissertation proposes optimal trajectories which include time-optimal trajectories and energy-saving ones. These trajectories are given in a closed form of explicit functions derived from solving analytically the nonlinear second order differential equation representing the translational motion of the vehicle. The dissertation also proposes a trajectory-tracking controller using sliding mode method. This controller can force the vehicle to track the designed trajectories very well, even with uncertainties. Its robustness can be guaranteed if bounds of the uncertainties are known.

The dissertation also presents the calculation of required thrust range of thruster(s) based on constraints of the optimal trajectories and robustness of the controller. Accordingly, thruster capacity can be chosen if related vehicle parameters and requirements of performance are identified.

The dissertation will focus on the case of depth motion control of the vehicle as an illustration for the proposed solutions. Similar ones could be made for other

directions of translational motion of the vehicle. The effectiveness of the proposed designs will be demonstrated via simulation results.

KEY WORDS: UUV, Optimal trajectory, Tracking controller, Depth control, , Thrust design, Sliding Mode Control, Uncertainty

Contents

Nomenclature

m	vehicle mass
p	roll rate (body-fixed reference frame)
q	pitch rate (body-fixed reference frame)
r	yaw rate (body-fixed reference frame)
u	surge velocity (body-fixed reference frame)
v	sway velocity (body-fixed reference frame)
w	heave velocity (body-fixed reference frame)
x_g	the body-fixed coordinate of the vehicle center of gravity on the surge axis
y_g	the body-fixed coordinate of the vehicle center of gravity on the sway axis
z_g	the body-fixed coordinate of the vehicle center of gravity on the heave axis
x	the x-component inertial coordinate of the vehicle
y	the y-component inertial coordinate of the vehicle
z	the z-component inertial coordinate of the vehicle
ϕ	roll angle (inertial reference frame)
θ	pitch angle (inertial reference frame)
ψ	yaw angle (inertial reference frame)
W	vehicle weight
B	vehicle buoyancy
pTM	positive thrust margin
nTM	negative thrust margin

List of Tables

List of Figures

Chapter 1

Introduction

1.1 Background

In recent years, a large number of studies on unmanned underwater vehicles (UUVs) have been published. However, studies on the optimal control, especially in topics of time-optimal and energy-efficient maneuvers, of such vehicles have been rare. They are still underdeveloped (*Chyba et al., 2008a*).

The most basic position controller is the regulator, whose input is a constant of desired position. This controller usually causes sudden changes and unexpected overshoots. The more advanced one is the trajectory-tracking controller, whose input is a time-varying position reference signal (trajectory). If the trajectory is well designed (smoothly and feasibly), this controller will perform well, making gradual changes and almost no overshoots. A simple trajectory can be the output of a low-pass filter, whose input is a constant of desired position, or a polynomial which smoothly connects the departure point with the destination (*Fraga et al., 2003*). Such trajectories can be easily designed. However, they may not have time optimality or energy efficiency. Recently, *Chyba et al.* presented a numerical method for designing the time-optimal trajectory (*Chyba et al., 2008b*) or the weighted consumption and time-optimal trajectory (*Chyba et al., 2008a*). The numerical method needs a nonlinear optimization solver, which requires discretizing state and control variables of a nonlinear optimization model before using an approximate calculation algorithm to find the time or/and consumption optimal trajectories. This method is quite complex and has some weaknesses. The calculation algorithm can only be implemented with a powerful processor and its results take a long time to converge. Because of an offline method, it restricts the controller's automatic ability. The designed optimal trajectories and control forces are given in the form of sequences of discrete values the storage of which requires a large memory. In addition, *Chyba et al.* (*2008a&b*) have not been interested in

developing a suitable controller which can help the vehicle track the desired trajectory. They presented open-loop controllers, whose inputs are the sequences of predetermined discrete values of control forces. Such controllers cannot ensure a good trajectory-tracking performance for the vehicle, as expected, because of the influence of uncertainties such as dynamic perturbations, and disturbances which always exist in the case of UUVs.

So, new approaches in finding the optimal trajectories, together with a robust tracking controller, are expected.

1.2 Motivation

The time-optimal or energy-efficient trajectories are essential to UUV maneuver. Such trajectories were given by *Chyba et al.* (*2008a&b*). However, they are the results of a numerical solver which is difficult to use. An analytical solution for this issue is expected, and is a new challenge.

1.3 Contributions

In this dissertation, an analytical method, not a numerical method, is used to find the optimal trajectories. They are explicit functions given in closed-form expressions, whose formats are unchanged. The use of such functions increases the controller's automatic ability. The proposed controller is a trajectory-tracking controller, so it offers time optimality or energy efficiency as long as its references (inputs) are the time-optimal or energy-efficient trajectories, respectively; even with uncertainties.

The dissertation also presents the calculation of required thrust range of thruster(s) based on constraints of the optimal trajectories and robustness of the controller. This thrust range is reference for engineers to decide thruster capacity for choosing thruster(s).

1.4 Methodology

In the dissertation, the analytical method is used to solve the nonlinear second order differential equation representing the translational motion for finding the optimal trajectories.

For a robust controller, the sliding mode method is used to design the trajectory-tracking controller.

1.5 Dynamics assumptions

The dynamic equations of UUV are used in the design process of the optimal trajectories. These dynamic equations are given with the following assumptions:

- The vehicle is deeply submerged in a homogeneous, unbounded fluid (the vehicle is located far from free surface – no surface effects).
- The effects of the vehicle passing through its own wake are ignored.
- The vehicle propeller is a source of constant thrust and its torque is small, thus ignored.

Chapter 2

Mathematical Model of Unmanned Underwater Vehicle

2.1 Body-fixed and inertial coordinate systems

A coordinate system fixed with the body of vehicle, called body-fixed coordinate system, with its origin set at the center of vehicle buoyancy, is used to describe dynamics of UUV. The motion of the body-fixed frame of reference is described relative to an inertial or earth-fixed reference frame as shown in Fig. 2.1.

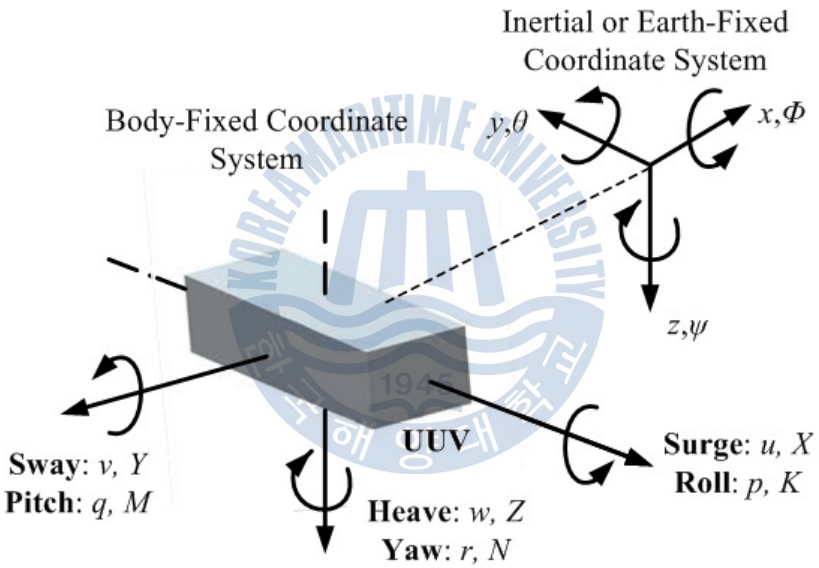

Figure 2.1 Body-fixed and inertial coordinate systems

2.2 Full equations of motion

2.2.1 Vehicle kinematics

As shown in Fig. 2.1, (x, y, z) and (ϕ, θ, ψ) are the position and orientation of the vehicle with respect to (wrt) the inertial reference frame respectively. The following coordinate transform relates translational velocities between body-fixed and inertial coordinates:

$$\begin{bmatrix} \dot{x} \\ \dot{y} \\ \dot{z} \end{bmatrix} = J_1(\eta) \begin{bmatrix} u \\ v \\ w \end{bmatrix} \tag{1}$$

where $\eta = (\phi, \theta, \psi)$

$$J_1(\eta) = \begin{bmatrix} \cos\psi\cos\theta & -\sin\psi\cos\phi + \cos\psi\sin\theta\sin\phi & \sin\psi\sin\phi + \cos\psi\sin\theta\cos\phi \\ \sin\psi\cos\theta & \cos\psi\cos\phi + \sin\psi\sin\theta\sin\phi & -\cos\psi\sin\phi + \sin\psi\sin\theta\cos\phi \\ -\sin\theta & \cos\theta\sin\phi & \cos\theta\cos\phi \end{bmatrix}$$

The second coordinate transform relates rotational velocities between body-fixed and inertial coordinates:

$$\begin{bmatrix} \dot{\phi} \\ \dot{\theta} \\ \dot{\psi} \end{bmatrix} = J_2(\eta) \begin{bmatrix} p \\ q \\ r \end{bmatrix} \tag{2}$$

where

$$J_2(\eta) = \begin{bmatrix} 1 & \sin\phi\tan\theta & \cos\phi\tan\theta \\ 0 & \cos\phi & -\sin\phi \\ 0 & \sin\phi/\cos\theta & \cos\phi/\cos\theta \end{bmatrix}$$

Note that $J_2(\eta)$ is not defined for pitch angle $\theta = \pm 90°$. This is not a problem as the vehicle motion does not ordinarily approach this singularity. If we were in a situation where it became necessary to model the vehicle motion through extreme pitch angles, we could resort to an alternate kinematic representation such as quaternions.

2.2.2 Vehicle rigid-body dynamics

Given that the origin of the body-fixed coordinate system is located at the center of buoyancy as noted in Section 2.1, the following represents the full equations of motion for a six degree-of-freedom rigid body in body-fixed coordinates (*Fossen, 1994*):

$$
\begin{aligned}
&m[\dot{u} - vr + wq - x_g(q^2 + r^2) + y_g(pq - \dot{r}) + z_g(pr + \dot{q})] = \sum X \\
&m[\dot{v} - wp + ur - y_g(r^2 + p^2) + z_g(qr - \dot{p}) + x_g(qp + \dot{r})] = \sum Y \\
&m[\dot{w} - uq + vp - z_g(p^2 + q^2) + x_g(rp - \dot{q}) + y_g(rq + \dot{p})] = \sum Z \\
&I_{xx}\dot{p} + (I_{zz} - I_{yy})qr - (\dot{r} + pq)I_{xz} + (r^2 - q^2)I_{yz} + (pr - \dot{q})I_{xy} \\
&\qquad + m[y_g(\dot{w} - uq + vp) - z_g(\dot{v} - wp + ur)] = \sum K \\
&I_{yy}\dot{q} + (I_{xx} - I_{zz})rp - (\dot{p} + qr)I_{xy} + (p^2 - r^2)I_{xz} + (qp - \dot{r})I_{yz} \\
&\qquad + m[z_g(\dot{u} - vr + wq) - x_g(\dot{w} - uq + vp)] = \sum M \\
&I_{zz}\dot{r} + (I_{yy} - I_{xx})pq - (\dot{q} + rp)I_{yz} + (q^2 - p^2)I_{xy} + (rq - \dot{p})I_{xz} \\
&\qquad + m[x_g(\dot{v} - wp + ur) - y_g(\dot{u} - vr + wq)] = \sum N
\end{aligned}
\tag{3}
$$

where

- u, v, w: surge, sway, heave velocities respectively
- p, q, r: roll, pitch, yaw rates (positive sense as in (Fig. 2.1)
- X, Y, Z: external forces
- K, M, N: external moments
- x_g, y_g, z_g: center of gravity wrt origin at center of buoyancy
- I_{ab}: moments of inertia wrt origin at center of buoyancy (a and b symbolize x or y or z)
- m: vehicle mass

$$
\begin{aligned}
\sum X &= X_{HS} + X_{u|u|}u\,|u| + X_{\dot{u}}\dot{u} + X_{wq}wq + X_{qq}qq + X_{vr}vr \\
&\quad + X_{rr}rr + X_{prop} \\
\sum Y &= Y_{HS} + Y_{v|v|}v\,|v| + Y_{r|r|}r\,|r| + Y_{\dot{v}}\dot{v} + Y_{\dot{r}}\dot{r} + Y_{ur}ur + Y_{wp}wp \\
&\quad + Y_{pq}pq + Y_{uv}uv + Y_{prop} \\
\sum Z &= Z_{HS} + Z_{w|w|}w\,|w| + Z_{q|q|}q\,|q| + Z_{\dot{w}}\dot{w} + Z_{\dot{q}}\dot{q} + Z_{uq}uq \\
&\quad + Z_{vp}vp + Z_{rp}rp + Z_{uw}uw + Z_{prop} \\
\sum K &= K_{HS} + K_{p|p|}p\,|p| + K_{\dot{p}}\dot{p} + K_{prop} \\
\sum M &= M_{HS} + M_{w|w|}w\,|w| + M_{q|q|}q\,|q| + M_{\dot{w}}\dot{w} + M_{\dot{q}}\dot{q} \\
&\quad + M_{uq}uq + M_{vp}vp + M_{rp}rp + M_{uw}uw + M_{prop} \\
\sum N &= N_{HS} + N_{v|v|}v\,|v| + N_{r|r|}r\,|r| + N_{\dot{v}}\dot{v} + N_{\dot{r}}\dot{r} + N_{ur}ur \\
&\quad + N_{wp}wp + N_{pq}pq + N_{uv}uv + N_{prop}
\end{aligned}
\tag{4}
$$

with the formulas of hydrostatic forces and moments:

$$
\begin{aligned}
X_{HS} &= -(W-B)\sin\theta \\
Y_{HS} &= (W-B)\cos\theta\sin\phi \\
Z_{HS} &= (W-B)\cos\theta\cos\phi \\
K_{HS} &= -y_g W\cos\theta\cos\phi - z_g W\cos\theta\sin\phi \\
M_{HS} &= -z_g W\sin\theta - x_g W\cos\theta\cos\phi \\
N_{HS} &= -x_g W\cos\theta\sin\phi - y_g W\sin\theta
\end{aligned}
\tag{5}
$$

here,

- $X_{prop}, Y_{prop}, Z_{prop}$: the thrusts of the thrusters projected on the corresponding axes
- $K_{prop}, M_{prop}, N_{prop}$: the steering moments made by the thrusters
- *W, B*: weight and buoyancy of the vehicle respectively
- The remaining factors are other nonlinear maneuvering coefficients of forces and moments (*Fossen, 1994*).

Equations (1)-(5) give out a mathematical model of UUV which provide a platform for vehicle control system development, and an alternative to the typical trial-and-error method of vehicle control system field tuning.

2.3 Depth plane model

In this dissertation, we just focus on the design and tracking control of optimal trajectories for the depth motion of the vehicle as an illustration for the proposed solutions, so we only need to consider the body-relative heave velocity w, and the earth-relative vehicle depth z. We will set all other translational and rotational velocities to zero, and assume that the roll, pitch and yaw angles of the vehicle always are kept at zero for simplicity. As a result, the mathematical model of the depth motion (depth plane model) of the vehicle is as follows:

$$(m - Z_{\dot{w}})\dot{w} - Z_{w|w|} w \mid w \mid = (W - B) + Z_{prop} \tag{6}$$

$$\dot{z} = w \tag{7}$$

Substituting Eq. (7) into (6), we have:

$$(m - Z_{\dot{w}})\ddot{z} - Z_{w|w|} \dot{z} \mid \dot{z} \mid = (W - B) + Z_{prop} \tag{8}$$

Setting $a = m - Z_{\dot{w}} > 0$, $b = -Z_{w|w|} > 0$, $N = B - W > 0$ (net buoyancy), and $u = Z_{prop}$, Eq. (8) becomes:

$$a\ddot{z} + b\dot{z} \mid \dot{z} \mid + N = u \tag{9}$$

Eq. (9) can be used as a reference model for generating the optimal depth trajectories if the values of the parameters a, b, N, u are given. In the next chapter, the optimal depth trajectories are designed by solving analytically Eq. (9), so are given in closed-form expressions.

Chapter 3

Optimal Trajectories

3.1 Time-optimal trajectories

For time-optimal trajectories (TOTs), our approach stems from the fact that the minimum time to destination can be attained when the thruster(s) of the vehicle always operates at maximum thrust levels during the maneuver. Therefore, the depth differential equation of the vehicle given in Eq. (9) with appropriate constant thrust forces will be solved to find the time-optimal trajectories.

We will design TOTs for the vehicle when it moves from the beginning depth z_0 at time t_0 ($z_0 = 0$, $t_0 = 0$) to the ending depth z_e at time t_e ($z_e > 0$). At both these depth levels, the vehicle is at rest, meaning that its velocity is zero ($\dot{z}(t_0) = v_0 = 0$, $\dot{z}(t_e) = v_e = 0$). Depending on the value of the ending depth z_e, there are two plans for the course of the vehicle velocity $\dot{z}$. Plan I: if z_e is large, $\dot{z}$ will increase from zero to the critical value v_m (acceleration period), and it will stay at this value for a certain period of time (constant velocity period), and then decrease to zero right at the ending time t_e (deceleration period). Plan II: if z_e is small, $\dot{z}$ will increase from zero to a certain value, not greater than v_m, (acceleration period), and then decrease to zero right at the ending time t_e (deceleration period). Plan II does not have the constant velocity period. In both plans mentioned above, the vehicle velocity is always non-negative. So, we can rewrite Eq. (9) as follows:

$$a\ddot{z} + b\dot{z}^2 + N = u \tag{10}$$

Setting net force $f = u - N$ (11)

Eq (10) becomes:

$$a\ddot{z} + b\dot{z}^2 = f \tag{12}$$

From Eq. (11), if we know the value of the net buoyancy N and the range of the

thrust force u, we can calculate the range of the net force f.

Assuming $f_1 \le f \le f_2$, with $f_1 < 0,\ f_2 > 0$, TOTs can be obtained by solving Eq. (12) either with $f = f_2$ (corresponding to $u = u_2$) for the constant velocity and acceleration periods or with $f = f_1$ (corresponding to $u = u_1$) for the deceleration period. Here, u_1 and u_2 are the designed constant thrust forces.

3.1.1 TOTs with the constant velocity and acceleration periods

Eq. (12) is rewritten as follows:

$$a\ddot{z}_d + b\dot{z}_d^2 = f_2 \tag{13}$$

The constraints for these periods are:

$$a,\ b,\ f_2 > 0 \quad \text{and} \quad \dot{z}_d\ ,\ \ddot{z}_d \ge 0 \tag{C1}$$

At the beginning time t_0, the initial conditions are:

- $\dot{z}_d(t=t_0=0) = v_0 = 0$ (K1)
- $z_d(t=t_0=0) = z_0 = 0$ (K2)

here, t denotes the variable of time.

Setting $\dot{z}_d = h(t) \ge 0$ (14)

we have:

$$\ddot{z}_d = \frac{dh(t)}{dt} \tag{15}$$

Substituting Eqs. (14) and (15) into Eq. (13) yields:

$$a\frac{dh}{dt} + b.h^2 = f_2 \tag{16}$$

Eq. (16) can be rewritten:

$$a\frac{dh}{dt} = f_2 - b.h^2 \tag{17}$$

- **If $f_2 - b.h^2 \neq 0$**

From Eq. (17), we have:

$$a\frac{dh}{f_2 - b.h^2} = dt$$

or, $$\frac{-a}{b}.\frac{dh}{h^2 - \frac{f_2}{b}} = dt \tag{18}$$

Finding the antiderivative of each function at both sides of Eq. (18), we obtain:

$$\frac{-a}{2\sqrt{b.f_2}}.\ln\left|1 - \frac{2\sqrt{f_2/b}}{h + \sqrt{f_2/b}}\right| = t + c_1 \tag{19}$$

* From Eq. (13), we have:

$b\dot{z}_d^2 = f_2 - a\ddot{z}_d \leq f_2$, due to $a > 0$ and $\ddot{z}_d \geq 0$ as stated at the constraints C1

or, $$h = \dot{z}_d \leq \sqrt{f_2/b} \tag{20}$$

Adding $\sqrt{f_2/b}$ to both sides of the inequality (20), we have:

$$h + \sqrt{f_2/b} \leq 2\sqrt{f_2/b}$$

or, $$1 - \frac{2\sqrt{f_2/b}}{h + \sqrt{f_2/b}} \leq 0 \tag{21}$$

From (19) & (21), we have:

$$\frac{-a}{2\sqrt{b.f_2}}.\ln\left(\frac{2\sqrt{f_2/b}}{h + \sqrt{f_2/b}} - 1\right) = t + c_1 \tag{22}$$

* From Eq. (22) and the condition (K1), we have:

$$c_1 = \frac{-a}{2\sqrt{b.f_2}}.\ln\left(\frac{2\sqrt{f_2/b}}{v_0+\sqrt{f_2/b}}-1\right)-t_0 \tag{23}$$

Eq. (22) can be rewritten as follows:

$$\ln\left(\frac{2\sqrt{f_2/b}}{h+\sqrt{f_2/b}}-1\right)=\frac{-2\sqrt{b.f_2}}{a}(t+c_1)$$

or, $$\dot{z}_d = h = \frac{2\sqrt{f_2/b}}{1+e^{\frac{-2\sqrt{b.f_2}}{a}(t+c_1)}}-\sqrt{f_2/b} \tag{24}$$

From Eq. (24), we can easily deduce the expression of $\ddot{z}_d$ as follows:

$$\ddot{z}_d = \frac{d\dot{z}_d}{dt} = \frac{4f_2}{a}.\frac{e^{\frac{-2\sqrt{b.f_2}}{a}(t+c_1)}}{\left(1+e^{\frac{-2\sqrt{b.f_2}}{a}(t+c_1)}\right)^2} \tag{25}$$

In addition, Eq. (24) can be written as follows:

$$dz_d = 2\sqrt{f_2/b}\frac{e^{\frac{2\sqrt{b.f_2}}{a}(t+c_1)}.dt}{1+e^{\frac{2\sqrt{b.f_2}}{a}(t+c_1)}}-\sqrt{f_2/b}.dt$$

or, $$dz_d = \frac{a}{b}.\frac{d\left(1+e^{\frac{2\sqrt{b.f_2}}{a}(t+c_1)}\right)}{1+e^{\frac{2\sqrt{b.f_2}}{a}(t+c_1)}}-\sqrt{f_2/b}.dt \tag{26}$$

Finding the antiderivative of each function at both sides of Eq. (26), we obtain:

$$z_d = \frac{a}{b}.\ln(1+e^{\frac{2\sqrt{b.f_2}}{a}(t+c_1)})-\sqrt{f_2/b}.t+c_2 \tag{27}$$

* From Eq. (27) and the condition (K2), we have:

$$c_2 = z_0 - \frac{a}{b}.\ln(1+e^{\frac{2\sqrt{b.f_2}}{a}(t_0+c_1)}) + \sqrt{f_2/b}.t_0 \tag{28}$$

- **If $f_2 - b.h^2 = 0$**, we have:

$$h^2 = \frac{f_2}{b}$$

or, $\dot{z}_d = h = \sqrt{f_2/b} = \text{constant}$ (29)

$\dot{z}_d = \sqrt{f_2/b}$ given in Eq. (29) is accepted if the initial time is denoted by t_1 instead of t_0, $t_1 \neq t_0$, and the following initial conditions are satisfied:

- $\dot{z}_d(t=t_1) = v_1 = \sqrt{\frac{f_2}{b}} = v_m$ (critical velocity) (K3)
- $z_d(t=t_1) = z_1$ (K4)

In fact, this is a particular case in which the velocity has reached the critical value. At this time, the net force is balanced with the drag force $b.\dot{z}_d^2$, the vehicle velocity no longer changes and stays at the critical velocity $\sqrt{f_2/b}$. So, the vehicle acceleration is zero and the vehicle depth increases linearly with time.

From Eq. (29) we easily obtain:

$$\begin{cases} \ddot{z}_d = 0 & (30) \\ z_d = \sqrt{f_2/b}.t + c_3 & (31) \end{cases}$$

* From Eq. (31) and the condition (K4), we have:

$$c_3 = z_1 - \sqrt{f_2/b}.t_1 \tag{32}$$

So, the solutions for z_d, $\dot{z}_d$, and $\ddot{z}_d$ satisfying Eq. (13) are as follows:

$$
\begin{cases}
\text{(I)} \begin{cases}
z_{d1}(t) = \dfrac{a}{b}.\ln\left(1+e^{\frac{2\sqrt{b.f_2}}{a}(t+c_1)}\right) - \sqrt{f_2/b}.t + c_2 & (27)\\
\dot{z}_{d1}(t) = \dfrac{2\sqrt{f_2/b}}{1+e^{\frac{-2\sqrt{b.f_2}}{a}(t+c_1)}} - \sqrt{f_2/b} & (24)\\
\ddot{z}_{d1}(t) = \dfrac{4f_2}{a}.\dfrac{e^{\frac{-2\sqrt{b.f_2}}{a}(t+c_1)}}{\left(1+e^{\frac{-2\sqrt{b.f_2}}{a}(t+c_1)}\right)^2} & (25)\\
c_1 = \dfrac{-a}{2\sqrt{b.f_2}}.\ln\left(\dfrac{2\sqrt{f_2/b}}{v_0+\sqrt{f_2/b}}-1\right) - t_0 & (23)\\
c_2 = z_0 - \dfrac{a}{b}.\ln\left(1+e^{\frac{2\sqrt{b.f_2}}{a}(t_0+c_1)}\right) + \sqrt{f_2/b}.t_0 & (28)
\end{cases}\\
\text{(II)} \begin{cases}
z_{d2}(t) = v_1.t + c_3 & (31)\\
\dot{z}_{d2}(t) = v_1 & (29)\\
\ddot{z}_{d2}(t) = 0 & (30)\\
c_3 = z_1 - v_1.t_1 & (32)
\end{cases}
\end{cases}
$$

3.1.2 TOTs with the deceleration period

Eq. (12) is similarly rewritten as follows:

$$a\ddot{z}_d + b\dot{z}_d^2 = f_1 \tag{33}$$

The constraints for this period are:

$$a,\ b > 0;\ f_1 < 0 \quad \text{and} \quad z_d \geq 0;\ \ddot{z}_d \leq 0 \tag{C2}$$

Assuming t_2 is the initial time of this period, the corresponding initial conditions are:

- $\dot{z}_d(t=t_2) = v_2 > 0$ (K5)
- $z_d(t=t_2) = z_2$ (K6)

Setting $\dot{z}_d = h(t) \geq 0$ (14)

we have:

$$\ddot{z}_d = \frac{dh(t)}{dt} \tag{15}$$

Substituting Eqs. (14) and (15) into Eq. (33) yields:

$$a\frac{dh}{dt} + b.h^2 = f_1 \tag{34}$$

Eq. (34) can be rewritten:

$$a\frac{dh}{dt} = f_1 - b.h^2 < 0 \tag{35}$$

($f_1 - b.h^2 < 0$ due to $f_1 < 0$ and $b > 0$ as stated at the constraints C2)

From Eq. (35), we have:

$$a\frac{dh}{f_1 - b.h^2} = dt$$

or, $$\frac{-a}{b}.\frac{dh}{h^2 + \frac{-f_1}{b}} = dt \tag{36}$$

Finding the antiderivative of each function at both sides of Eq. (36), we obtain:

$$\frac{-a}{\sqrt{-b.f_1}}.\arctan\left(\frac{h}{\sqrt{-f_1/b}}\right) = t + c_4 \tag{37}$$

* From Eq. (37) and the condition (K5), we have:

$$c_4 = \frac{-a}{\sqrt{-b.f_1}}.\arctan\left(\frac{v_2}{\sqrt{-f_1/b}}\right) - t_2 \tag{38}$$

Eq. (37) can be written as follows:

$$\arctan\left(\frac{h}{\sqrt{-f_1/b}}\right)=\frac{-\sqrt{-b.f_1}}{a}.(t+c_4)$$

$$\text{or,}\quad \dot{z}_d=h=\sqrt{\frac{-f_1}{b}}\tan\left(\frac{-\sqrt{-b.f_1}}{a}.(t+c_4)\right) \tag{39}$$

From Eq. (39), we can easily deduce the expression of $\ddot{z}_d$ as follows:

$$\ddot{z}_d=\frac{d\dot{z}_d}{dt}=\frac{f_1}{a}.\frac{1}{\cos^2\left(\frac{-\sqrt{-b.f_1}}{a}.(t+c_4)\right)} \tag{40}$$

In addition, Eq. (39) can be written as follows:

$$dz_d=\sqrt{-f_1/b}\tan\left(\frac{-\sqrt{-b.f_1}}{a}.(t+c_4)\right).dt$$

$$\text{or,}\quad dz_d=\frac{a}{b}.\frac{d\left[\cos\left(\frac{-\sqrt{-b.f_1}}{a}.(t+c_4)\right)\right]}{\cos\left(\frac{-\sqrt{-b.f_1}}{a}.(t+c_4)\right)} \tag{41}$$

Finding the antiderivative of each function at both sides of Eq. (41), we obtain:

$$z_d=\frac{a}{b}.\ln\left|\cos\left(\frac{-\sqrt{-b.f_1}}{a}.(t+c_4)\right)\right|+c_5 \tag{42}$$

* From Eq. (42) and the condition (K6), we have:

$$c_5=z_2-\frac{a}{b}.\ln\left|\cos\left(\frac{-\sqrt{-b.f_1}}{a}.(t_2+c_4)\right)\right| \tag{43}$$

So, the solutions for z_d, $\dot{z}_d$, and $\ddot{z}_d$ satisfying Eq. (33) are as follows:

$$
\text{(III)}\begin{cases}
z_{d3}(t) = \dfrac{a}{b}.\ln\left|\cos\left(\dfrac{-\sqrt{-b.f_1}}{a}.(t+c_4)\right)\right| + c_5 & (42)\\
\dot{z}_{d3}(t) = \sqrt{\dfrac{-f_1}{b}}\tan\left(\dfrac{-\sqrt{-b.f_1}}{a}.(t+c_4)\right) & (39)\\
\ddot{z}_{d3}(t) = \dfrac{f_1}{a}.\dfrac{1}{\cos^2\left(\dfrac{-\sqrt{-b.f_1}}{a}.(t+c_4)\right)} & (40)\\
c_4 = \dfrac{-a}{\sqrt{-b.f_1}}.\arctan\left(\dfrac{v_2}{\sqrt{-f_1/b}}\right) - t_2 & (38)\\
c_5 = z_2 - \dfrac{a}{b}.\ln\left|\cos\left(\dfrac{-\sqrt{-b.f_1}}{a}.(t_2+c_4)\right)\right| & (43)
\end{cases}
$$

3.1.3 The profiles of the TOTs

For Plan I:

TOTs of Plan I (Plan I trajectories) have shapes as shown in Fig. 3.1. They are used when the ending deph z_e has a large value (long range) satisfying the inequality below.

$$z_e > z_e^*$$

where $$z_e^* = z_1^* + \Delta z_3^* \quad (44)$$

z_1^*: the distance travelled during the period from the initial time t_0 to the time t_1^* when the vehicle velocity just reaches the critical value v_1^* (or v_m) as shown in Fig. 3.1c and 3.1d. During this period, the net force f is always kept at the high level f_2, and the vehicle acceleration decreases from the maximum value f_2/a to zero as shown in Fig. 3.1b.

Δz_3^*: the distance travelled during the period from the time when the vehicle velocity starts decreasing from the critical value v_m to the ending time t_e when it just falls to zero as shown in Fig. 3.1c and 3.1d. During this period, the net force f is always kept at the low level f_1, and the vehicle acceleration increases from the peak negative value $(f_1 - b.v_m^2)/a$ to a smaller negative value of f_1/a as shown in

Fig. 3.1b.

Plan I trajectories can be divided into four segments in a sequence as follows:

– Segment I (the time is from t_0 to t_1): The net force f is always at the high level f_2. The acceleration decreases from the maximum value f_2/a to zero. The velocity increases from v_0 to v_1^*. And, the depth increases from z_0 to z_1^*. In this segment, the expressions of the TOTs are given as in system (I), including Eqs. (23-25, 27, 28). The initial and final velocity and depth states are (v_0, z_0) and (v_1, z_1), respectively. Note: $t_1 = t_1^*$, $v_1 = v_1^*$ (or v_m), $z_1 = z_1^*$.

– Segment II (the time from t_1 to t_2): The net force f is still at the high level f_2. The acceleration is zero. The velocity is always at v_m. And, the depth increases from z_1 to z_2. The corresponding expressions of the TOTs are given as in system (II), including Eqs. (29-32). The initial and final velocity and depth states are (v_1, z_1) and (v_2, z_2), respectively. Note: $v_1 = v_2 = v_m$.

– Segment III (the time from t_2 to t_3): The net force f is changed to the low level f_1 (the thruster(s) is assumed to be able to instantly change its thrust force from u_2 to u_1 corresponding to the change of the net force from f_2 to f_1, respectively). The acceleration instantly changes from zero (at the final point of segment II) to the peak negative value $(f_1 - b.v_m^2)/a$ (at the initial point of segment III), and then, increases to a smaller negative value of f_1/a as shown in Fig. 3.1b. The velocity decreases from v_m to zero. And, the depth increases from z_2 to z_e. The corresponding expressions of the TOTs are given as in system (III), including Eqs. (38-40, 42, 43). The initial and final velocity and depth states are (v_2, z_2) and (v_3, z_3), respectively. Note: $t_3 = t_e$, $v_3 = v_e = 0$, $z_3 = z_e$, $z_3 - z_2 = \Delta z_3^*$.

– Segment IV (the time from t_3 onwards): The net force f is zero. The acceleration instantly changes to zero and stays at this value. The velocity is also zero to keep the depth constant.

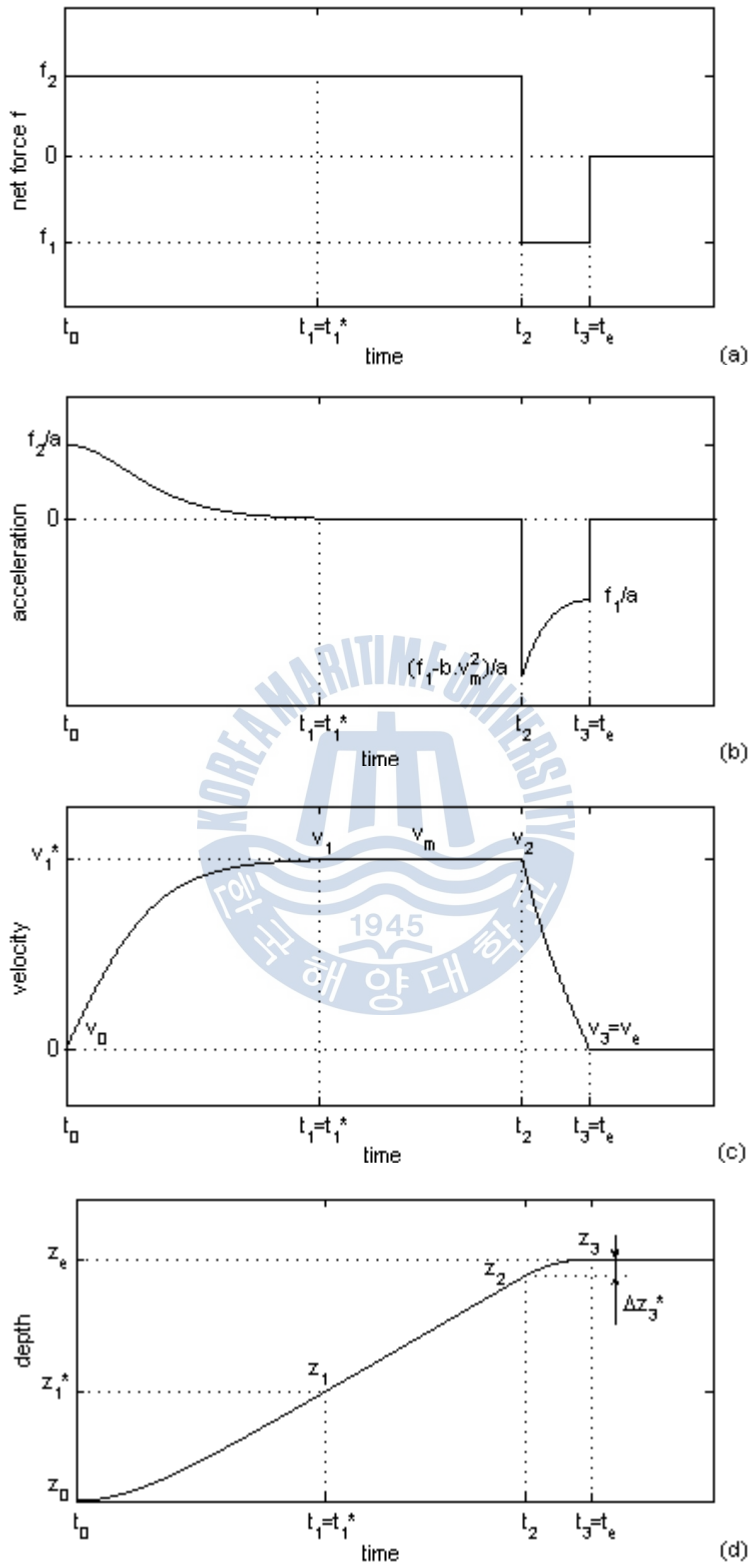

Fig. 3.1 Time-optimal trajectories of Plan I

The initial and final times, velocities, and depths of each segment are given or calculated as follows:

- t_0, v_0, z_0, v_e, z_e are given (t_0, v_0, z_0, $v_e = 0$)

  $$z_e > z_e^* = z_1^* + \Delta z_3^*$$

  The expression of z_1^* is given in Eq. (51) and the one of Δz_3^* given in Eq. (66).

- t_1, v_1, z_1

  To determine the value of the time t_1^* we should rely on the expression of the velocity $\dot{z}_{d1}$ shown in Eq. (24). As mentioned previously, the velocity reaches the critical value v_1^* at t_1^* So, we have:

  $$\dot{z}_{d1}(t_1^*) = v_1^* \tag{45}$$

  From Eqs (24) & (45), we have:

  $$\frac{2\sqrt{f_2/b}}{1+e^{\frac{-2\sqrt{b.f_2}}{a}(t_1^*+c_1)}} - \sqrt{f_2/b} = v_1^*$$

  or, $$t_1^* = \frac{-a}{2\sqrt{b.f_2}} \ln\left(\frac{\sqrt{f_2/b} - v_1^*}{\sqrt{f_2/b} + v_1^*}\right) - c_1 \tag{46}$$

  If the value of v_1^* is known, t_1^* can be determined by Eq. (46). Unfortunately, however, it is impossible get the value of t_1^* when v_1^* in Eq. (46) is replaced by $v_m = \sqrt{f_2/b}$ as expected. Indeed, this equation shows that t_1^* tends to infinity as v_1^* goes to v_m. It is similar to what happens in Eq. (24): the velocity $\dot{z}_{d1}$ converges to the critical value v_m as the time t goes to infinity. Fig. 3.1c shows, in the early stage of segment I, the velocity increases rapidly. But, when the velocity is closer to the critical value, its rate of increase is slower (the acceleration is smaller). The reason is that the cross-flow drag $b\dot{z}_d^2$ increases

proportionally to the square of velocity. So, the resultant force which includes the cross-flow drag and the net force becomes smaller when the velocity increases, and the acceleration also smaller as shown in Fig. 3.1b. As a result, the velocity increases slower. Mathematically, the velocity reaches the critical value at the time of infinity. This does not occur in reality. It is true that the velocity increases slower in the later stage of segment I, but it must attain the critical value after a limited period of time. This contradiction derives from the mathematical model, presented in *Fossen* (*1994*), which is used to describe the motion behaviors of the UUV. Being verified by experiments, the model is said to reflect the relationship among the states of the vehicle in the best way, but this does not mean that it accurately reflects what actually happens. On the other hand, perhaps the current mathematical tools such as functions or operators are still not able to describe the essence of this relationship in which the velocity reaches the critical value after a limited period of time, not approach it. However, the model does not lose its representation because of this problem, but it is still the means by which we come closest to the actual behaviors of the UUV. Our concern now is how to use it properly.

Note that, according to the mathematical model, there is a very narrow neighbourhood of the critical value v_m, denoted δ_v, in which the velocity converges extremely slowly. This neighbourhood does not exist in reality, so we need to determine and eliminate it. Here, the upper limit of δ_v is chosen equal to the critical value v_m, and its lower limit is $\xi.v_m$.

$$\delta_v = [\xi.v_m \quad v_m] \tag{47}$$

where $\xi < 1$ and $\xi \approx 1$

The value of ξ is chosen so that the time when the velocity, in the mathematical model, reaches $\xi.v_m$ is equal to the time when the velocity, in reality, reaches v_m. That time is t_1^*. And, the value of ξ should be verified by experiments.

So, to calculate t_1^* by Eq. (46), we should choose:

$$v_1^* = \xi.v_m = \xi.\sqrt{f_2 / b} \approx v_m \tag{48}$$

Substituting Eq. (48) into Eq. (46) yields:

$$t_1 = t_1^* = \frac{-a}{2.\sqrt{b.f_2}}.\ln\left(\frac{1-\xi}{1+\xi}\right) - c_1 \tag{49}$$

And, we have:

$$v_1 = v_1^* = \xi.v_m \tag{50}$$

$$z_1 = z_1^* = z_{d1}(t_1^*) \tag{51}$$

- t_2, v_2, z_2

In segment II, the distance travelled is $(z_e - z_e^*)$, the velocity is constant v_m. So, the time for the vehicle to pass over this distance is $(z_e - z_e^*)/v_m$. Therefore, we have:

$$t_2 = t_1^* + \frac{z_e - z_e^*}{v_m} \tag{52}$$

$$v_2 = v_m \tag{53}$$

$$z_2 = z_e - \Delta z_3^* \tag{54}$$

- t_3, v_3, z_3

The velocity is zero at t_3. So, we have:

$$\dot{z}_{d3}(t_3) = 0 \tag{55}$$

From Eqs. (39) and (55), we obtain:

$$\sqrt{\frac{-f_1}{b}}\tan\left(\frac{-\sqrt{-b.f_1}}{a}.(t_3 + c_4)\right) = 0$$

or, $t_3 = t_e = -c_4$ (56)

And, we have:

$$v_3 = v_e = 0 \tag{57}$$

$$z_3 = z_e \tag{58}$$

Find Δz_3^*:

The depth is z_e at t_3. So, we have:

$$z_{d3}(t_3) = z_e \tag{59}$$

From Eqs. (42) and (59), we obtain:

$$\frac{a}{b}.\ln\left|\cos\left(\frac{-\sqrt{-b.f_1}}{a}.(t_3 + c_4)\right)\right| + c_5 = z_e \tag{60}$$

Substituting the expression of t_3 given in Eq. (56) into Eq. (60) yields:

$$c_5 = z_e \tag{61}$$

Then, replacing c_5 in Eq. (61) by its expression given in Eq. (43):

$$z_2 - \frac{a}{b}.\ln\left|\cos\left(\frac{-\sqrt{-b.f_1}}{a}.(t_2 + c_4)\right)\right| = z_e \tag{62}$$

Next, replacing c_4 in Eq. (62) by its expression given in Eq. (38):

$$z_2 - \frac{a}{b}.\ln\left|\cos\left(\arctan\left(\frac{v_2}{\sqrt{-f_1/b}}\right)\right)\right| = z_e \tag{63}$$

We have the relationship between trigonometric function *cos* and inverse trigonometric function *arctan* as follows:

$$\cos(\arctan x) = \frac{1}{\sqrt{1+x^2}} \tag{64}$$

So, Eq. (63) can be rewritten as follows:

$$z_2 - \frac{a}{b}.\ln\left(1\Big/\sqrt{1+\frac{v_2^2}{-f_1/b}}\right) = z_e \tag{65}$$

Therefore, we have:

$$\Delta z_3^* = z_e - z_2 = \frac{-a}{b}.\ln\left(1\Big/\sqrt{1+\frac{v_m^2}{-f_1/b}}\right) \tag{66}$$

For Plan II:

If $z_e \le z_e^*$ (short range), Plan II trajectories, as shown in Fig. 3.2, will be used. Plan II trajectories can be divided into three segments in a sequence as follows:

– Segment I (the time is from t_0 to t_1): The net force f is always at the high level f_2. The acceleration decreases from the maximum value f_2/a to a certain non-negative value, as shown in Fig. 3.2b. The velocity increases from v_0 to v_1. And the depth increases from z_0 to z_1. In this segment, the expressions of the TOTs are also given as in system (I), including Eqs. (23-25, 27, 28). The initial and final velocity and depth states are (v_0, z_0) and (v_1, z_1), respectively.

– Segment II (the time from t_1 or t_2 to t_3): The net force f is changed to the low level f_1. The acceleration instantly changes from the non-negative value (at the final point of segment I) to a peak negative value (at the initial point of segment II), and then, increases to a smaller negative value of f_1/a as shown in Fig. 3.2b. The velocity decreases from v_1 to zero. And, the depth increases from z_1 to z_e. The corresponding expressions of the TOTs are given as in system (III), including Eqs. (38-40, 42, 43). The initial and final velocity and depth states are (v_1, z_1) or (v_2, z_2), and (v_3, z_3), respectively. Note: $t_1 = t_2$, $v_1 = v_2$, $z_1 = z_2$, $t_3 = t_e$, $v_3 = v_e = 0$, $z_3 = z_e$.

– Segment III (the time from t_3 onwards): The net force f is zero. The acceleration instantly changes to zero and stays at this value. The velocity is also zero.

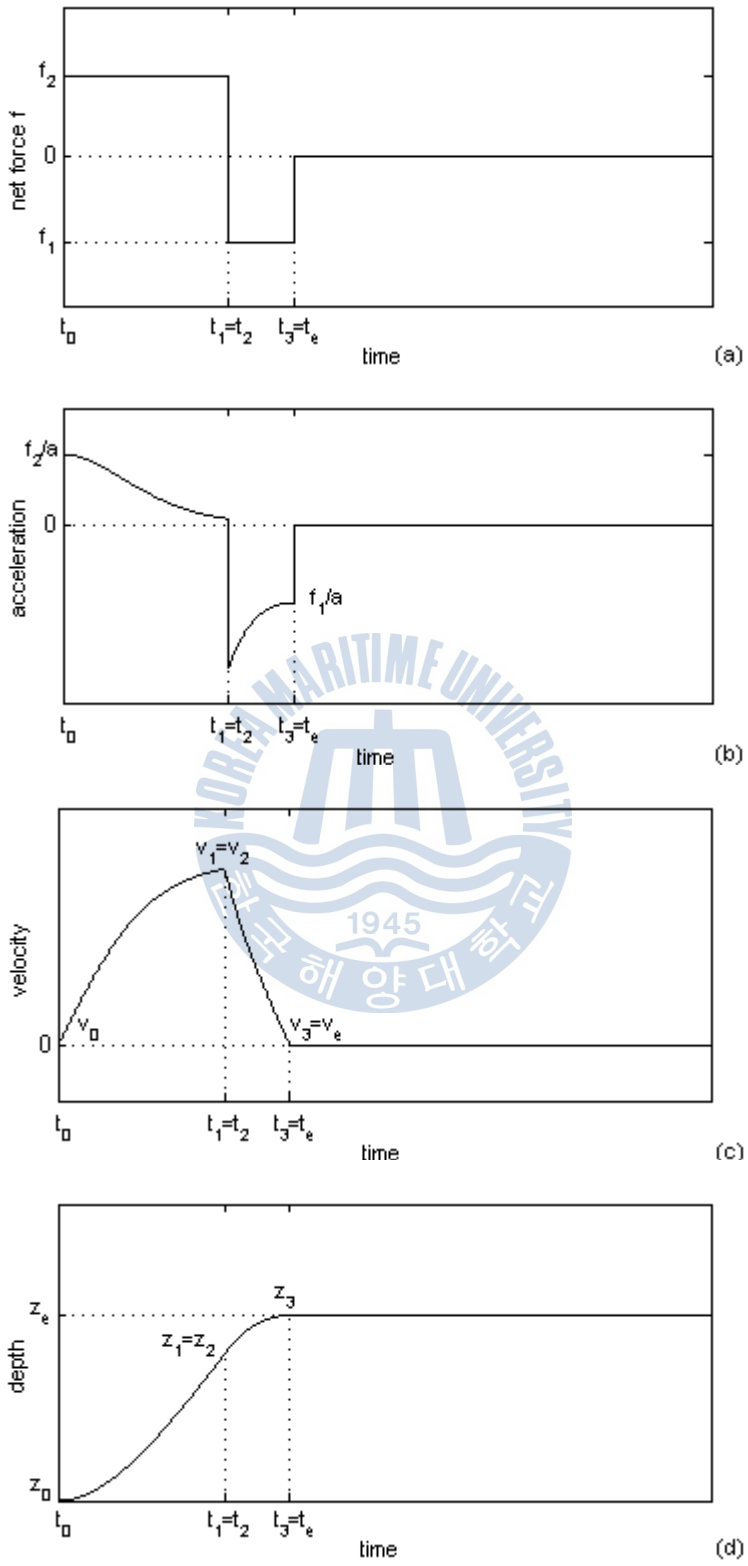

Fig. 3.2 Time-optimal trajectories of Plan II

The initial and final times, velocities, and depths of each segment are given or calculated as follows:

- t_0, v_0, z_0, v_e, z_e are given (t_0, v_0, z_0, $v_e = 0$)

  $z_e \le z_e^*$

- t_1, v_1, z_1 or t_2, v_2, z_2 and t_3, v_3, z_3

  The expressions of t_1, v_1, z_1, and t_3 are solutions of the following system of equations:

$$\begin{cases} z_{d1}(t_1) = z_1 = z_2 & (67) \\ \dot{z}_{d1}(t_1) = v_1 = v_2 & (68) \\ z_{d3}(t_3) = z_e & (59) \\ \dot{z}_{d3}(t_3) = 0 & (55) \end{cases}$$

From Eqs. (27) and (67), we have:

$$\frac{a}{b}.\ln\left(1+e^{\frac{2\sqrt{b.f_2}}{a}(t_1+c_1)}\right)-\sqrt{f_2/b}.t_1+c_2 = z_1 \quad (69)$$

From Eqs. (24) and (68), we obtain:

$$\frac{2\sqrt{f_2/b}}{1+e^{\frac{-2\sqrt{b.f_2}}{a}(t_1+c_1)}}-\sqrt{f_2/b} = v_1$$

$$\text{or,}\quad v_1 = \sqrt{f_2/b}.\frac{-1+e^{\frac{2\sqrt{b.f_2}}{a}(t_1+c_1)}}{1+e^{\frac{2\sqrt{b.f_2}}{a}(t_1+c_1)}} \quad (70)$$

Similar to the previous part (for Plan I), Eqs. (55) and (59) lead to Eqs. (56) and (65) as follows:

$$t_3 = t_e = -c_4 = \frac{a}{\sqrt{-b.f_1}}.\arctan\left(\frac{v_2}{\sqrt{-f_1/b}}\right)+t_2 \quad (56)$$

or, $t_3 = \frac{a}{\sqrt{-b.f_1}}.\arctan\left(\frac{v_1}{\sqrt{-f_1/b}}\right) + t_1$ (71)

(due to $t_1 = t_2$ and $v_1 = v_2$)

$$z_2 - \frac{a}{b}.\ln\left(1\Big/\sqrt{1+\frac{v_2^2}{-f_1/b}}\right) = z_e \quad (65)$$

or, $z_1 = z_e + \frac{a}{b}.\ln\left(1\Big/\sqrt{1+\frac{v_1^2}{-f_1/b}}\right)$ (72)

(due to $z_1 = z_2$ and $v_1 = v_2$)

Now, the expressions of t_1, v_1, z_1, and t_3 are solutions of a new system of equations as follows:

$$\begin{cases} \frac{a}{b}.\ln(1+e^{\frac{2\sqrt{b.f_2}}{a}(t_1+c_1)}) - \sqrt{f_2/b}.t_1 + c_2 = z_1 & (69) \\ v_1 = \sqrt{f_2/b}.\frac{-1+e^{\frac{2\sqrt{b.f_2}}{a}(t_1+c_1)}}{1+e^{\frac{2\sqrt{b.f_2}}{a}(t_1+c_1)}} & (70) \\ z_1 = z_e + \frac{a}{b}.\ln\left(1\Big/\sqrt{1+\frac{v_1^2}{-f_1/b}}\right) & (72) \\ t_3 = \frac{a}{\sqrt{-b.f_1}}.\arctan\left(\frac{v_1}{\sqrt{-f_1/b}}\right) + t_1 & (71) \end{cases}$$

Substituting the expression of z_1 given in Eq. (72) into Eq. (69) yields:

$$\frac{a}{b}.\ln(1+e^{\frac{2\sqrt{b.f_2}}{a}(t_1+c_1)}) - \sqrt{f_2/b}.t_1 + c_2 = z_e + \frac{a}{b}.\ln\left(1\Big/\sqrt{1+\frac{v_1^2}{-f_1/b}}\right)$$

or, $\ln\left(\sqrt{1+\frac{v_1^2}{-f_1/b}}.\left(1+e^{\frac{2\sqrt{b.f_2}}{a}(t_1+c_1)}\right)\right) = \frac{b}{a}.(\sqrt{f_2/b}.t_1 + z_e - c_2)$

Taking the exponential of both sides, we have:

$$\sqrt{1+\frac{v_1^2}{-f_1/b}}.\left(1+e^{\frac{2\sqrt{b.f_2}}{a}.(t_1+c_1)}\right)=e^{\frac{\sqrt{b.f_2}}{a}.(t_1+c_1)}.e^{\frac{b}{a}.(z_e-c_2-\sqrt{f_2/b}.c_1)}$$

Then, squaring both sides, we obtain:

$$\left(1+\frac{v_1^2}{-f_1/b}\right).\left(1+e^{\frac{2\sqrt{b.f_2}}{a}.(t_1+c_1)}\right)^2=e^{\frac{2\sqrt{b.f_2}}{a}.(t_1+c_1)}.e^{\frac{2b}{a}.(z_e-c_2-\sqrt{f_2/b}.c_1)} \quad (73)$$

Replacing v_1 in Eq. (73) by its expression given in Eq. (70) yields:

$$\left(1+\frac{f_2}{-f_1}.\frac{\left(-1+e^{\frac{2\sqrt{b.f_2}}{a}(t_1+c_1)}\right)^2}{\left(1+e^{\frac{2\sqrt{b.f_2}}{a}(t_1+c_1)}\right)^2}\right).\left(1+e^{\frac{2\sqrt{b.f_2}}{a}.(t_1+c_1)}\right)^2=e^{\frac{2\sqrt{b.f_2}}{a}.(t_1+c_1)}.e^{\frac{2b}{a}.(z_e-c_2-\sqrt{f_2/b}.c_1)}$$

or, $$\left(1+e^{\frac{2\sqrt{b.f_2}}{a}.(t_1+c_1)}\right)^2+\frac{f_2}{-f_1}.\left(-1+e^{\frac{2\sqrt{b.f_2}}{a}.(t_1+c_1)}\right)^2=e^{\frac{2\sqrt{b.f_2}}{a}.(t_1+c_1)}.e^{\frac{2b}{a}.(z_e-c_2-\sqrt{f_2/b}.c_1)} \quad (74)$$

Set: $$x=e^{\frac{2\sqrt{b.f_2}}{a}.(t_1+c_1)}>1 \quad (75)$$

Because t_0 and v_0 are assumed to be zero, c_1 defined in Eq. (23) is zero.

$$c_1=0 \quad (76)$$

a is greater than zero (C2). And it is obvious that t_1 must be greater than zero. So, $\frac{2\sqrt{b.f_2}}{a}.(t_1+c_1)>0$. Therefore, $e^{\frac{2\sqrt{b.f_2}}{a}.(t_1+c_1)}>1$.

$$\gamma = \frac{f_2}{-f_1} > 0, \qquad \text{due to } f_2, (-f_1) > 0 \tag{77}$$

$$h = e^{\frac{2b}{a}.(z_e - c_2 - \sqrt{f_2/b}.c_1)} > 4 \tag{78}$$

Because t_0 and z_0 are assumed to be zero, and c_1 is zero as shown in Eq. (76), c_2 defined in Eq. (28) has the following value:

$$c_2 = -\frac{a}{b}\ln 2 \tag{79}$$

So, $e^{\frac{2b}{a}.(z_e - c_2 - \sqrt{f_2/b}.c_1)} = e^{\frac{2b}{a}.(z_e + \frac{a}{b}\ln 2)} = 4.e^{\frac{2b}{a}.z_e} > 4$

Note: With the values of t_0, v_0, z_0 given, we deduce the values of c_1 and c_2 as shown in Eqs. (76) and (79). However, we still keep the notation c_1 and c_2 in forthcoming expressions instead of their true values to maintain the generality of solutions for future reference.

Using the notation x, γ, h defined above for Eq. (74) yields:

$$(x+1)^2 + \gamma.(x-1)^2 = h.x$$

or, $$x^2 - 2.\frac{\gamma + h/2 - 1}{\gamma + 1}.x + 1 = 0 \tag{80}$$

The quadratic equation above has two roots as follows:

$$x_1 = \frac{\gamma + 0.5h - 1}{\gamma + 1} + \sqrt{\left(\frac{\gamma + 0.5h - 1}{\gamma + 1}\right)^2 - 1}$$

$$x_2 = \frac{\gamma + 0.5h - 1}{\gamma + 1} - \sqrt{\left(\frac{\gamma + 0.5h - 1}{\gamma + 1}\right)^2 - 1} \qquad \text{(rejected)}$$

x_2 is rejected because its value is less than 1. It does not satisfy the inequality (75). This is demonstrated as follows:

Set $n = \dfrac{\gamma + 0.5h - 1}{\gamma + 1} > 1$ (81)

n can be written as follows:

$$n = \frac{(\gamma+1) + 0.5h - 2}{\gamma + 1} = 1 + \frac{0.5h - 2}{\gamma + 1}$$

Due to $h > 4$ as shown in Eq. (78) we have $0.5h - 2 > 0$. We also have $\gamma > 0$ as shown in Eq. (77), so $\dfrac{0.5h-2}{\gamma+1} > 0$. As a result, $n = 1 + \dfrac{0.5h-2}{\gamma+1} > 1$.

Now, we have: $x_2 = n - \sqrt{n^2 - 1}$ (82)

Because n is greater than 1, we have the following chain of inequalities:

$$n > 1$$

$$-n < -1$$

$$-2n < -2$$

$$-2n + 1 < -1$$

$$n^2 - 2n + 1 < n^2 - 1$$

$$(n-1)^2 < n^2 - 1$$

$$n - 1 < \sqrt{n^2 - 1}$$

$$n - \sqrt{n^2 - 1} < 1$$

So, $x_2 = n - \sqrt{n^2 - 1} < 1$ (rejected)

Thus, the root of the equation (80) is as follows:

$$x = x_1 = n + \sqrt{n^2 - 1} = \frac{\gamma + 0.5h - 1}{\gamma + 1} + \sqrt{\left(\frac{\gamma + 0.5h - 1}{\gamma + 1}\right)^2 - 1} \tag{83}$$

After getting the value of x as shown in Eq. (83), we can calculate the value of t_1 as below.

Eq. (75) is rewritten:

$$x = e^{\frac{2\sqrt{b.f_2}}{a}.(t_1 + c_1)} \tag{75}$$

Taking the logarithm to the base e on both sides of the above equation yields:

$$\ln x = \frac{2\sqrt{b.f_2}}{a}.(t_1 + c_1)$$

$$\text{or, } t_1 = \frac{a}{2\sqrt{b.f_2}} \ln x - c_1 \tag{84}$$

Therefore, t_1, v_1, z_1, or t_2, v_2, z_2, and t_3, v_3, z_3 can be calculated sequentially as follows:

$$\gamma = \frac{f_2}{-f_1} \tag{77}$$

$$h = e^{\frac{2b}{a}.(z_e - c_2 - \sqrt{f_2/b}.c_1)} \tag{78}$$

$$n = \frac{\gamma + 0.5h - 1}{\gamma + 1} \tag{81}$$

$$x = x_1 = n + \sqrt{n^2 - 1} \tag{83}$$

$$t_1 = t_2 = \frac{a}{2\sqrt{b.f_2}} \ln x - c_1 \tag{84}$$

$$v_1 = v_2 = \sqrt{f_2 / b}.\frac{-1+e^{\frac{2\sqrt{b.f_2}}{a}(t_1+c_1)}}{1+e^{\frac{2\sqrt{b.f_2}}{a}(t_1+c_1)}} \tag{70}$$

$$z_1 = z_2 = \frac{a}{b}.\ln(1+e^{\frac{2\sqrt{b.f_2}}{a}(t_1+c_1)}) - \sqrt{f_2 / b}.t_1 + c_2 \tag{69}$$

$$t_3 = t_e = \frac{a}{\sqrt{-b.f_1}}.\arctan\left(\frac{v_1}{\sqrt{-f_1 / b}}\right) + t_1 \tag{71}$$

$$v_3 = v_e = 0 \tag{57}$$

$$z_3 = z_e \tag{58}$$

3.2 Energy-saving trajectories

In this section, we just discuss energy-saving trajectories (ESTs) applied for driving the vehicle in mode of moving down. Because the vehicle buoyancy is usually made slightly greater than the vehicle weight (the positive net buoyancy, N = B - W > 0, allows the vehicle to float to the surface in the event of a failure), in mode of moving up, the best energy-saving control way is to turn off all the thrusters and let the vehicle float slowly to the desired position.

For energy-saving trajectories, our approach stems from using a thrust force at which the efficiency of thruster(s) is maximum, named the energy-efficient thrust force; and from an energy-efficient control strategy in which the accumulated kinetic energy of vehicle will be fully utilized in motion control, i.e., the thruster(s) is not used to brake the vehicle velocity during the maneuver.

Accordingly, in the constant velocity and acceleration periods, the thruster(s) will operate at the energy-efficient thrust force, denoted $u_2^{'}$, to save energy. The corresponding net force is $f_2^{'}$.

$$f_2^{'} = u_2^{'} - N \tag{85}$$

In the case of TOTs, the thrust force u is equal to u_2, whose value is chosen as large

as possible to achieve a high velocity, in order to shorten the travel time. However, in this case, the thrust force u is equal to the energy-efficient thrust force $u_2^{'}$, whose value is usually less than u_2. So, the vehicle velocity is smaller, the travel time is longer. In return, the energy consumption is lower.

In the deceleration period, our control strategy is not to use the reverse thrust force u_1 to brake the vehicle velocity as in the case of TOTs. Instead, the thruster(s) will stop operating; and the vehicle, with the kinetic energy accumulated in the previous period, will drift to the destination without propulsion. This strategy saves energy significantly. Indeed, in the case of TOTs, the vehicle is propelled at a high velocity, and comes very close to the destination before entering the deceleration period. This way helps the vehicle move quickly to the destination; however, it obliges the vehicle to use a high reverse force (u_1) to brake the velocity quickly in the deceleration period, in order to stop right at the destination at the end of this period. This method brings the benefit of saving time, but wastes energy. It could not utilize the accumulated kinetic energy, but also spend more energy to eliminate it – a double waste. Here, in the case of ESTs, the vehicle starts the deceleration period when it is quite far from the destination. Without any thrust force, the vehicle velocity will decrease due to the resistance of the cross-flow drag and the positive net buoyancy, it is expected to be equal to zero as soon as the vehicle arrives at the destination. The thrust force in this period $u_1^{'}$ is zero, so the corresponding net force $f_1^{'}$ is as follows:

$$f_1^{'} = u_1^{'} - N = -N \tag{86}$$

$$\text{due to} \quad u_1^{'} = 0 \tag{87}$$

With the use of the energy-efficient thrust force and control strategy as presented above, the travel time is longer; in return, the energy consumption is minimized. The expressions of ESTs (z_d, $\dot{z}_d$, $\ddot{z}_d$), and the formulas of milestones ($t_{1,2,3}$) and states ($v_{1,2,3}$; $z_{1,2,3}$) are similar to the ones in the case of TOTs, respectively; except to replace f_1 with $f_1^{'}$, and f_2 with $f_2^{'}$.

Chapter 4

Trajectory-Tracking Control

In this section, we present the depth trajectory-tracking control of the UUV and the design of trajectory-tracking controller using the sliding mode method.

4.1 Trajectory-tracking control

The depth trajectory-tracking control can be described by the control system block diagram shown in Fig. 4.1. In this diagram, the block *UUV* contains the model of the vehicle, and the model of thruster(s) (actuator) is ignored. The inputs of the block *Trajectory Generator* are the beginning and ending velocities and depths. This block calculates the optimal trajectories and sends them to the block *Trajectory-Tracking Controller*. The feedback signals of the vehicle states such as the acceleration, velocity, and depth are also sent to the block *Trajectory-Tracking Controller*. This block contains our controller which determines the control force u required to drive the vehicle for tracking the desired trajectories.

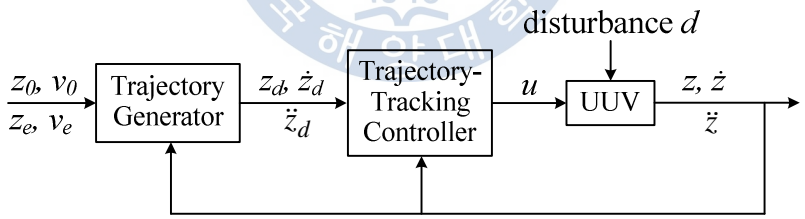

Fig. 4.1 UUV depth control system block diagram

4.2 Trajectory-tracking controller

As mentioned, the range of the net force f, which is used to design the optimal trajectories, is determined from the value of the net buoyancy N and the desired range of the thrust force (from u_1 or u_1' to u_2 or u_2'). So, to have a good performance, a well-designed trajectory-tracking controller should require a control

force whose value is always within that desired range. This issue is a priority in our design.

With the sliding mode method, when there are no uncertainties, the control force is maintained within the desired range which is used to design the optimal trajectories; otherwise, it may be outside the desired range. So, the thruster(s) should be chosen to have appropriated thrust margins such that it can meet the potential maximum commands of the control force; in other words the maximum forward thrust force of the thruster(s) should be greater than the maximum forward control force required by the controller, and similarly the maximum reverse thrust force should be greater than the maximum reverse control force (in absolute form). The difference between the maximum forward or reverse thrust force of the thruster(s) and the designed thrust force u_2 or u_1 (in absolute form) is denoted as the positive or negative thrust margin, respectively. The values of these margins depend on the parameters of the controller, the dynamics of the vehicle, the dynamics of the thruster(s), and the shapes of the designed trajectories (smooth and feasible or not). These margins will be presented in detail in the next chapter.

In tracking control, another issue to be considered is the effects of uncertainties, which include dynamic perturbations (unstructured and parametric uncertainties) and disturbances (underwater current,…), on the performance of the controller. They greatly affect its robustness. A trajectory-tracking controller without robustness to uncertainties will fail in its tracking mission. In this dissertation, we use the sliding mode method to design the trajectory-tracking controller because it can provide the controller with the robustness in dealing with uncertainties.

The mathematical model of depth motion of the UUV with uncertainties is as follows:

$$a\ddot{z} + b\dot{z}\,|\,\dot{z}\,| + N = u + d \tag{88}$$

In Eq. (88), a, b, N are parametric uncertainties, estimated as

$\hat{a}$, $\hat{b}$, $\hat{N}$, respectively; d is disturbance. Their bounds and values are defined as follows:

$$a_{\min} \le a \le a_{\max},\ \hat{a} = \frac{(a_{\max} + a_{\min})}{2},\ \Delta a = \frac{(a_{\max} - a_{\min})}{2}, \tag{89}$$

$$b_{\min} \le b \le b_{\max},\ \hat{b} = \frac{(b_{\max} + b_{\min})}{2},\ \Delta b = \frac{(b_{\max} - b_{\min})}{2}, \tag{90}$$

$$-D \le d \le D,\ \hat{d} = 0,\ \Delta d = D \ge 0,\ N_{\min} \le N \le N_{\max}, \tag{91}$$

$$\hat{N} = \frac{(N_{\max} + N_{\min})}{2},\ \Delta N = \frac{(N_{\max} - N_{\min})}{2} \tag{92}$$

4.2.1 Sliding mode control law

The sliding mode method is based on the idea of keeping the scalar quantity s, which is a weighted sum of the position error $(z - z_d)$, the velocity error $(\dot{z} - \dot{z}_d)$, and (not required) the acceleration error $(\ddot{z} - \ddot{z}_d)$, at zero (*Slotine and Li, 1991*):

$$s = 0 \tag{93}$$

Here, the expression of s is chosen as in Eq. (94):

$$s = (\dot{z} - \dot{z}_d) + \lambda(z - z_d) \tag{94}$$

where $\lambda > 0$ is the weight parameter

Therefore, the task of the controller is to take s to zero. And, when s approaches zero, position error (and velocity error, also) approaches zero too, and thus, trajectory-tracking is performed.

Once s is zero, to keep it at this value, the derivative of s is expected to be zero:

$$\dot{s} = 0 \tag{95}$$

From Eq. (94), we can easily deduce the expression of $\dot{s}$ as follows:

$$\dot{s} = (\ddot{z} - \ddot{z}_d) + \lambda(\dot{z} - \dot{z}_d) \tag{96}$$

From Eq. (88), the expression of $\ddot{z}$ is:

$$\ddot{z} = \frac{1}{a}.(-b.\dot{z}\,|\,\dot{z}\,| - N + u + d) \tag{97}$$

Substituting Eq. (97) into Eq. (96) yields:

$$\dot{s} = \frac{1}{a}.(-b.\dot{z}\,|\,\dot{z}\,| - N + u + d) - \ddot{z}_d + \lambda(\dot{z} - \dot{z}_d) \tag{98}$$

So, if $\dot{s} = 0,$ we have:

$$\frac{1}{a}.(-b.\dot{z}\,|\,\dot{z}\,| - N + u + d) - \ddot{z}_d + \lambda(\dot{z} - \dot{z}_d) = 0$$

or, $u = b.\dot{z}\,|\,\dot{z}\,| + N + a.\ddot{z}_d - \lambda a.(\dot{z} - \dot{z}_d) - d$ (99)

From Eq. (99), the best approximation $\hat{u}$ of a continuous control law that would achieve $\dot{s} = 0$ is as follows:

$$\hat{u} = \hat{b}.\dot{z}\,|\,\dot{z}\,| + \hat{N} + \hat{a}.\ddot{z}_d - \lambda\hat{a}.(\dot{z} - \dot{z}_d) \tag{100}$$

And, the actual control law which can be robust to uncertainties is a discontinuous function chosen as follows:

$$\begin{aligned} u &= \hat{u} - K.\mathrm{sgn}(s) \\ &= \hat{b}.\dot{z}\,|\,\dot{z}\,| + \hat{N} + \hat{a}.\ddot{z}_d - \lambda.\hat{a}.(\dot{z} - \dot{z}_d) - K.\mathrm{sgn}(s) \end{aligned} \tag{101}$$

where, *sgn(.)* is the *signnum* function, defined as follows:

$$\mathrm{sgn}(s) = \begin{cases} 1 & \text{if } s > 0 \\ 0 & \text{if } s = 0 \\ -1 & \text{if } s < 0 \end{cases} \tag{102}$$

K is the design parameter chosen so that:

$$\dot{s}.s \leq -\eta |s| < 0 \tag{103}$$

where η is a strictly positive constant

4.2.2 Design parameter *K*

The condition (103) is given to ensure that the vehicle is always driven towards the states at which s is zero. Indeed, because $\dot{s}.s$ is always negative as required in (103), if s is a positive value, $\dot{s}$ must be negative, meaning that s is decreasing to 0; conversely, if s is a negative value, $\dot{s}$ must be positive, meaning that s is increasing to 0. Here, we will show how to choose K so that the condition (103) is satisfied.

Substituting Eq. (101) into Eq. (98) yields:

$$\dot{s} = \frac{\hat{b}-b}{a}.\dot{z}|\dot{z}| + \left(\frac{\hat{a}}{a}-1\right)\left[\ddot{z}_d - \lambda(\dot{z}-\dot{z}_d)\right] + \frac{1}{a}(\hat{N}-N) + \frac{d}{a} - \frac{K}{a}.\mathrm{sgn}(s) \tag{104}$$

Then, substituting Eq. (104) into the inequality (103), and noting that $s.\mathrm{sgn}(s) = |s|$, we have:

$$-\eta|s| \geq \left[\frac{\hat{b}-b}{a}.\dot{z}|\dot{z}| + \left(\frac{\hat{a}}{a}-1\right)\left[\ddot{z}_d - \lambda(\dot{z}-\dot{z}_d)\right] + \frac{1}{a}(\hat{N}-N) + \frac{d}{a}\right].s - \frac{K}{a}.|s| \tag{105}$$

Moving the term $K|s|$ of the inequality (105) to the left hand side and rearranging the terms lead to:

$$K|s| \geq \left[(\hat{b}-b).\dot{z}|\dot{z}| + (\hat{a}-a)\left[\ddot{z}_d - \lambda(\dot{z}-\dot{z}_d)\right] + (\hat{N}-N) + d\right].s + \eta.a|s| \tag{106}$$

It is easy to realize that the inequality (106) is always satisfied if K verifies:

$$K \geq \left|(\hat{b}-b).\dot{z}\,|\,\dot{z}\,|+(\hat{a}-a)\left[\ddot{z}_d-\lambda(\dot{z}-\dot{z}_d)\right]+(\hat{N}-N)+d\right|+\eta.a \tag{107}$$

From Eqs. (89-92), we have $\Delta b \geq |\hat{b}-b|$, $\Delta a \geq |\hat{a}-a|$, $\Delta N \geq |\hat{N}-N|$, and $D \geq |d|$. These in turn lead to:

$$K \geq \Delta b.\dot{z}^2+\Delta a.\left|\ddot{z}_d-\lambda(\dot{z}-\dot{z}_d)\right|+\Delta N+D+\eta.a_{\max} \tag{108}$$

So, our sliding mode controller is designed as given in Eq. (101) with K chosen by (108). To avoid chattering by the use of the *signnum* function *sgn(.)*, we can replace the *signnum* function with the *saturating* function as follows:

$$\text{sat}(s/\phi)=\begin{cases}\text{sgn}(s/\phi) & \text{if } |s/\phi|>1\\ s/\phi & \text{otherwise}\end{cases} \tag{109}$$

where $\phi > 0$ is the boundary layer thickness.

Chapter 5

Thrust Design

5.1 Normal thrust

This section presents how to calculate the thrust forces required to take the vehicle to destination with a given travel time. This is an inverse problem which gives us distance and travel time, and asks about the required thrust forces. It is applied for designing the normal thrust which is the normal operating point of thruster(s) when there are no uncertainties.

We will use criterion of optimal time as a platform for calculating these forces. This means that we will use the results of Section 3.1 to calculate the normal thrusts which turn out to be the thrust forces u_1 and u_2. The criterion of time optimality is chosen instead of the one of the energy efficiency because the range $[u_1 \;\; u_2]$ covers the range $[u_1' \;\; u_2']$.

The problem is stated as follows: Calculate the thrust forces u_1 and u_2 required to drive the vehicle from the depth of zero to the depth z_e with the travel time t_e, according to the criterion of optimal time. Assume that $z_e \geq z_e^*$; and t_0, v_0, z_0, $v_e = 0$ and the ratio $\gamma = f_2/(-f_1)$ is given.

Solution:

Set $$\Delta t_3^* = t_e - t_2 \tag{110}$$

Find Δt_3^*:

Eq. (56) is rewritten:

$$t_3 = t_e = -c_4 = \frac{a}{\sqrt{-b.f_1}}.\arctan\left(\frac{v_2}{\sqrt{-f_1/b}}\right) + t_2 \tag{56}$$

So, we have:

$$\Delta t_3^* = t_e - t_2 = \frac{a}{\sqrt{-b.f_1}}.\arctan\left(\frac{v_2}{\sqrt{-f_1/b}}\right)$$

or, $\Delta t_3^* = a.\sqrt{\frac{\gamma}{b.f_2}}.\arctan\left(\sqrt{\gamma}\right)$ (111)

due to $-f_1 = f_2/\gamma$ and $v_2 = v_m = \sqrt{f_2/b}$

Find t_1^*:

Eq. (49) is rewritten:

$$t_1^* = \frac{-a}{2.\sqrt{b.f_2}}.\ln\left(\frac{1-\xi}{1+\xi}\right) - c_1 \quad (49)$$

From Eq. (76), we have $c_1 = 0$. So, we obtain:

$$t_1^* = \frac{-a}{2.\sqrt{b.f_2}}.\ln\left(\frac{1-\xi}{1+\xi}\right) \quad (112)$$

Find z_e^*:

From Eqs. (27) and (51), we have:

$$z_1^* = \frac{a}{b}.\ln(1+e^{\frac{2\sqrt{b.f_2}}{a}(t_1^*+c_1)}) - \sqrt{f_2/b}.t_1^* + c_2 \quad (113)$$

Replacing t_1^* in Eq. (113) by its expressions given in Eq. (112); and replacing c_1 and c_2 in Eq. (113) by their values given in Eqs. (76) and (79) yields:

$$z_1^* = \frac{a}{b}.\ln\left(\frac{1}{\sqrt{1-\xi^2}}\right) \quad (114)$$

Eq. (66) is rewritten:

$$\Delta z_3^* = \frac{-a}{b}.\ln\left(1\Big/\sqrt{1+\frac{v_m^2}{-f_1/b}}\right) \quad (66)$$

or, $\Delta z_3^* = \frac{a}{b}.\ln\left(\sqrt{1+\gamma}\right)$ (115)

due to $-f_1 = f_2/\gamma$ and $v_2 = v_m = \sqrt{f_2/b}$

Eq. (44) is rewritten:

$$z_e^* = z_1^* + \Delta z_3^* \tag{44}$$

Substituting Eqs. (114-115) into Eq. (44), we obtain:

$$z_e^* = \frac{a}{b}.\ln\left(\sqrt{\frac{1+\gamma}{1-\xi^2}}\right) \tag{116}$$

Find f_2 and f_1:

We easily recognize that:

$$t_2 + \Delta t_3^* = t_e \tag{117}$$

Replacing t_2 in Eq. (117) by its expression given in (52) yields:

$$t_1^* + \Delta t_3^* + \frac{z_e - z_e^*}{v_m} = t_e$$

$$\text{or,}\quad t_1^* + \Delta t_3^* + \frac{z_e - z_e^*}{\sqrt{f_2 / b}} = t_e \tag{118}$$

$$\text{due to} \qquad v_m = \sqrt{f_2 / b}$$

Then, substituting Eqs. (111), (112) and (116) into Eq. (118):

$$\frac{-a}{2.\sqrt{b.f_2}}.\ln\left(\frac{1-\xi}{1+\xi}\right) + a.\sqrt{\frac{\gamma}{b.f_2}}.\arctan\left(\sqrt{\gamma}\right) + \frac{z_e - \frac{a}{b}.\ln\left(\sqrt{\frac{1+\gamma}{1-\xi^2}}\right)}{\sqrt{f_2 / b}} = t_e$$

$$\text{or,}\quad f_2 = \frac{\left[a.\ln\left(\frac{1+\xi}{\sqrt{1+\gamma}}\right) + a.\sqrt{\gamma}.\arctan\left(\sqrt{\gamma}\right) + b.z_e\right]^2}{b.t_e^2} \tag{119}$$

And then, we can calculate f_1 as follows:

$$f_1 = \frac{-f_2}{\gamma} \tag{120}$$

Find u_1 and u_2:

After having the expressions of the net forces f_2 and f_1 as given in Eqs. (119) and (112), we easily calculate the thrust forces as below:

$$u_1 = f_1 + N \tag{121}$$

$$u_2 = f_2 + N \tag{122}$$

5.2 Thrust margin

Back to the optimal trajectories, the estimated parameters $\hat{a}$, $\hat{b}$, and $\hat{N}$; instead of a, b, and N which are parametric uncertainties; will be used in Eq.s (23-25), (27-28), (38-40) and (42-43).

From Eq. (11), the designed net force f_d can be rewritten as follows:

$$f_d = u_d - \hat{N} \tag{123}$$

where u_d is the designed thrust force

According to the conventions presented in Section 3.1, $u_d = u_2$ corresponding to $f_d = f_2$ for the constant velocity and acceleration periods, and $u_d = u_1$ corresponding to $f_d = f_1$ for the deceleration period. So, from Eqs. (13), (33) and (123), we obtain Eqs. (124-126) as follows:

$$u_1 = \hat{a}.\ddot{z}_{d3} + \hat{b}.\dot{z}_{d3}^2 + \hat{N} \tag{124}$$

$$u_2 = \hat{a}.\ddot{z}_{d1} + \hat{b}.\dot{z}_{d1}^2 + \hat{N} \tag{125}$$

or, $$u_2 = \hat{a}.\ddot{z}_{d2} + \hat{b}.\dot{z}_{d2}^2 + \hat{N} \tag{126}$$

With the controller designed as given at Eq. (101), if there are no uncertainties; i.e., a, b and N are exactly equal to $\hat{a}$, $\hat{b}$ and $\hat{N}$, respectively, and d is zero; the control force u will be approximately equal to u_2 and u_1 in the relevant periods. However, if the uncertainties exist, the control force u will have to be greater than u_2, and less than u_1 to be able to achieve a good tracking performance.

Assuming that $[u_l \quad u_h]$ is the thrust range of thruster(s), u_{max} and u_{min} are the maximum and minimum values of the control force required by the controller, we have the following relationships:

$$u_h \geq u_{\max} > u_2 > 0 \qquad \text{and} \qquad 0 > u_1 > u_{\min} \geq u_l \tag{127}$$

So, it is necessary to find the values of u_l and u_h satisfying the inequality (127) because they are used to choose the thruster capacity.

Set $$pTM = u_h - u_2 \tag{128}$$

$$nTM = u_l - u_1 \tag{129}$$

pTM and *nTM* are positive and negative thrust margins, respectively, we will do estimate these margins as presented below.

From here onwards, the function *sat(s/ϕ)* is used, instead of the function *sign(s)*, for the controller given at Eq. (101) to avoid chattering; and the parameter K is chosen as the following:

$$K = \Delta b.\dot{z}^2 + \Delta a.\left|\ddot{z}_d - \lambda(\dot{z} - \dot{z}_d)\right| + \Delta N + D + \eta.a_{\max} \tag{130}$$

(see the inequality (108))

5.2.1 Positive thrust margin *pTM*:

In this section, we will find the formula of *pTM*. From Eq. (109), we have the following inequality:

$$\text{sat}(s/\phi) \geq -1 \tag{131}$$

Multiplying both sides by -1, we have:

$$-\text{sat}(s/\phi) \le 1$$

Then, multiplying both sides by K, we obtain:

$$-K.\text{sat}(s/\phi) \le K$$

Next, adding both sides by $\hat{u}$ yields:

$$\hat{u} - K.\text{sat}(s/\phi) \le \hat{u} + K$$

Due to $u = \hat{u} - K.\text{sat}(s/\phi)$, the above inequality becomes:

$$u \le \hat{u} + K \tag{132}$$

Substituting the expressions of $\hat{u}$ and K given in Eqs. (100) and (130) into the inequality (132):

$$\begin{aligned} u \le\ & \hat{b}.\dot{z}\,|\,\dot{z}\,| + \hat{N} + \hat{a}.\ddot{z}_d - \lambda.\hat{a}.(\dot{z} - \dot{z}_d) \\ & + \Delta b.\dot{z}^2 + \Delta a.\left|\ddot{z}_d - \lambda(\dot{z} - \dot{z}_d)\right| + \Delta N + D + \eta.a_{\max} \end{aligned}$$

Due to $\dot{z}\,|\,\dot{z}\,| \le \dot{z}^2$, the following inequality can cover the above:

$$\begin{aligned} u \le\ & \hat{b}.\dot{z}^2 + \Delta b.\dot{z}^2 + \hat{a}.\ddot{z}_d - \lambda.\hat{a}.(\dot{z} - \dot{z}_d) \\ & + \Delta a.\left|\ddot{z}_d - \lambda(\dot{z} - \dot{z}_d)\right| + \hat{N} + \Delta N + D + \eta.a_{\max} \end{aligned}$$

Due to $\hat{b} + \Delta b = b_{\max}$ and $\hat{N} + \Delta N = N_{\max}$, we have:

$$\begin{aligned} u \le\ & b_{\max}.\dot{z}^2 + \hat{a}.\ddot{z}_d - \lambda.\hat{a}.(\dot{z} - \dot{z}_d) \\ & + \Delta a.\left|\ddot{z}_d - \lambda(\dot{z} - \dot{z}_d)\right| + N_{\max} + D + \eta.a_{\max} \end{aligned} \tag{133}$$

It is easy to realize that the control force can only get the maximum value in the constant velocity and acceleration periods. So, we only need to consider the inequality (133) with the trajectories $\ddot{z}_d$, $\dot{z}_d$ designed for segments I and II. As a result, $\ddot{z}_d$ is non-negative. Due to $\lambda > 0$, it is easy to realize that the right hand side of the inequality (133) gets greater when the velocity error $(\dot{z} - \dot{z}_d)$ is non-positive.

Therefore, we could only consider the below constraints:

$$u \le b_{\max}.\dot{z}^2 + \hat{a}.\ddot{z}_d - \lambda.\hat{a}.(\dot{z} - \dot{z}_d) + \Delta a.\left|\ddot{z}_d - \lambda(\dot{z} - \dot{z}_d)\right| + N_{\max} + D + \eta.a_{\max} \quad (133)$$

with $\ddot{z}_d = \ddot{z}_{d1}$ or $\ddot{z}_{d2} \ge 0$, $\dot{z}_d = \dot{z}_{d1}$ or $\dot{z}_{d2} \ge 0$, $(\dot{z} - \dot{z}_d) \le 0$, $\lambda > 0$ (134)

From the constraints (134), we deduce $\ddot{z}_d - \lambda(\dot{z} - \dot{z}_d) \ge 0$. So, $\left|\ddot{z}_d - \lambda(\dot{z} - \dot{z}_d)\right| = \ddot{z}_d - \lambda(\dot{z} - \dot{z}_d)$. The inequality (133) becomes:

$$u \le b_{\max}.\dot{z}^2 + (\hat{a} + \Delta a).\ddot{z}_d - \lambda.(\hat{a} + \Delta a).(\dot{z} - \dot{z}_d) + N_{\max} + D + \eta.a_{\max}$$

or, $$u \le b_{\max}.\dot{z}^2 + a_{\max}.\ddot{z}_d - \lambda.a_{\max}.(\dot{z} - \dot{z}_d) + N_{\max} + D + \eta.a_{\max} \quad (135)$$

due to $\hat{a} + \Delta a = a_{\max}$

The term $\dot{z}^2$ is equivalent to $\left[(\dot{z} - \dot{z}_d) + \dot{z}_d\right]^2$. So, the inequality (135) can be rewritten as follows:

$$u \le b_{\max}.[(\dot{z} - \dot{z}_d) + \dot{z}_d]^2 + a_{\max}.\ddot{z}_d - \lambda.a_{\max}.(\dot{z} - \dot{z}_d) + N_{\max} + D + \eta.a_{\max}$$

or, $$u \le a_{\max}.\ddot{z}_d + b_{\max}.\dot{z}_d{}^2 + N_{\max} + b_{\max}.(\dot{z} - \dot{z}_d)^2 - (\lambda.a_{\max} - 2b_{\max}.\dot{z}_d).(\dot{z} - \dot{z}_d) + D + \eta.a_{\max} \quad (136)$$

From Eqs. (125-126) and (134), we have:

$$u_2 = \hat{a}.\ddot{z}_d + \hat{b}.\dot{z}_d^2 + \hat{N} \quad (137)$$

Then, from Eqs. (136-137), we deduce:

$$u \le \Delta a.\ddot{z}_d + \Delta b.\dot{z}_d{}^2 + b_{\max}.(\dot{z} - \dot{z}_d)^2 - (\lambda.a_{\max} - 2b_{\max}.\dot{z}_d).(\dot{z} - \dot{z}_d) + u_2 + \Delta N + D + \eta.a_{\max} \quad (138)$$

From Eq. (109), we have $|\mathrm{sat}(s/\phi)| \le 1$. So, if the designed trajectories are

smooth (no step changes) and feasible, and the parameter K is chosen so that the inequality (103) is satisfied, we can expect that the scalar quantity s will be bounded as in the following inequality:

$$|s| \le \phi \tag{139}$$

$$\text{or, } |(\dot{z}-\dot{z}_d)+\lambda(z-z_d)| \le \phi \tag{140}$$

If we set:

$$(\dot{z}-\dot{z}_d) = \rho.\phi \tag{141}$$

ρ is also bounded as follows:

$$|\rho| \le \mu, \text{ with } \mu > 0 \text{ (see Section 5.2.3)} \tag{142}$$

Substituting Eq. (141) into the inequality (138), we obtain:

$$u \le \Delta a.\ddot{z}_d + \Delta b.\dot{z}_d{}^2 + b_{\max}.\phi^2.\rho^2 - (\lambda.a_{\max} - 2b_{\max}.\dot{z}_d).\phi.\rho + u_2 + \Delta N + D + \eta.a_{\max} \tag{143}$$

with $-\mu \le \rho \le 0$, due to $(\dot{z}-\dot{z}_d) \le 0$ and $|\rho| \le \mu$ from the constraints (134) and (142)

The sliding mode controller tries to reduce the scalar quantity s, which is a weighted sum of the position error $(z-z_d)$, and the velocity error $(\dot{z}-\dot{z}_d)$, with the weight λ as given in Eq. (94). So, if the smaller the position error is required, the greater the weight λ should be chosen. As a result, the term $(\lambda.a_{\max} - 2b_{\max}.\dot{z}_d)$ is usually non-negative. So, the right hand side of the inequality (143) gets the maximum value when $\rho = -\mu$.

- **If $(\lambda.a_{\max} - 2b_{\max}.\dot{z}_d) \ge 0$**

As discussed above, replacing ρ by $-\mu$ in the inequality (143), we have a new inequality which can cover the old as follows:

$$u \le \Delta a.\ddot{z}_d + \Delta b.\dot{z}_d{}^2 + b_{\max}.\phi^2.\mu^2 + (\lambda.a_{\max} - 2b_{\max}.\dot{z}_d).\phi.\mu + u_2 + \Delta N + D + \eta.a_{\max} \quad (144)$$

Set $g_{h1} = \Delta a.\ddot{z}_d + \Delta b.\dot{z}_d{}^2 - 2\mu\phi b_{\max}.\dot{z}_d$ (145)

From Eqs. (144) and (145), we should choose:

$$u_h = \max(g_{h1}) + u_2 + \Delta N + D + \eta.a_{\max} + \mu.\phi.\lambda.a_{\max} + \mu^2.\phi^2.b_{\max} \quad (146)$$

where $\max(g_{h1})$ is the maximum value of the function g_{h1}.

So, we get the formula of *pTM* as follows:

$$pTM = u_h - u_2 = \max(g_{h1}) + \Delta N + D + \eta.a_{\max} + \mu.\phi.\lambda.a_{\max} + \mu^2.\phi^2.b_{\max} \quad (147)$$

The function g_{h1} or $g_{h1}(t)$, which is a function of the time t, can get the maximum value at one of the following values of time t:

$$t = \begin{cases} t_{h1}^1 = 0 & (148) \\ t_{h1}^2 = t_2, \text{ with } t_2 > t_1^* & (149) \\ t_{h1}^3 = \left\{ t \;\middle|\; \dfrac{dg_{h1}}{dt} = 0,\ t > 0 \right\} & (150) \end{cases}$$

In fact, the expressions of $\ddot{z}_{d1}$ and $\dot{z}_{d1}$ will become the expressions of $\ddot{z}_{d2}$ and $\dot{z}_{d2}$ when $t > t_1^*$. So, for finding t_{h1}^3 as required at Eq. (150), we only need to replace $\ddot{z}_d$ and $\dot{z}_d$ in the function $g_{h1}(t)$ by the expressions of $\ddot{z}_{d1}$ and $\dot{z}_{d1}$, respectively. As a result, we have:

$$t_{h1}^3 = \frac{-\hat{a}}{2\sqrt{\hat{b}.f_2}}.\ln\left(\frac{\Delta a.\sqrt{\hat{b}.f_2} - \Delta b.\hat{a}.\sqrt{\dfrac{f_2}{\hat{b}}} + \mu.\phi.\hat{a}.b_{\max}}{\Delta a.\sqrt{\hat{b}.f_2} - \Delta b.\hat{a}.\sqrt{\dfrac{f_2}{\hat{b}}} - \mu.\phi.\hat{a}.b_{\max}} \right) - c_1 \quad (151)$$

So, $\max(g_{h1}) = \max\left\{g_{h1}(t_{h1}^1), g_{h1}(t_{h1}^2), g_{h1}(t_{h1}^3)\right\}$ (152)

- **If $(\lambda.a_{\max} - 2b_{\max}.\dot{z}_d) \geq 0$**

The term $(\lambda.a_{\max} - 2b_{\max}.\dot{z}_d)$ could turn negative at great values of the vehicle velocity $\dot{z}_d$. In this case, we set:

$$g_{h2} = \Delta a.\ddot{z}_d + \Delta b.\dot{z}_d{}^2 + b_{\max}.\phi^2.\rho^2 - (\lambda.a_{\max} - 2b_{\max}.\dot{z}_d).\phi.\rho \quad (153)$$

From Eqs. (143) and (153), we should choose:

$$u_h = \max(g_{h2}) + u_2 + \Delta N + D + \eta.a_{\max} \quad (154)$$

where max(g_{h2}) is the maximum value of the function g_{h2}.

So, we get the formula of *pTM* as follows:

$$pTM = u_h - u_2 = \max(g_{h2}) + \Delta N + D + \eta.a_{\max} \quad (155)$$

The function g_{h2} or $g_{h2}(t,\rho)$, which is a function of two variables t and ρ, can get the maximum value at one of the following points:

$$(t,\rho)=\begin{cases}(t_{h2}^1,\rho_{h2}^1)=(0,0);\ (t_{h2}^2,\rho_{h2}^2)=(t_2,0)\\ (t_{h2}^3,\rho_{h2}^3)=(0,-\mu);\ (t_{h2}^4,\rho_{h2}^4)=(t_2,-\mu)\\ (t_{h2}^5,\rho_{h2}^5)=(0,\rho)\ \Big|\ \dfrac{dg_{h2}(0,\rho)}{d\rho}=0,\ 0>\rho>-\mu\\ (t_{h2}^6,\rho_{h2}^6)=(t_2,\rho)\ \Big|\ \dfrac{dg_{h2}(t_2,\rho)}{d\rho}=0,\ 0>\rho>-\mu\\ (t_{h2}^7,\rho_{h2}^7)=(t,0)\ \Big|\ \dfrac{dg_{h2}(t,0)}{dt}=0,\ 0>t>t_2\\ (t_{h2}^8,\rho_{h2}^8)=(t,-\mu)\ \Big|\ \dfrac{dg_{h2}(t,-\mu)}{dt}=0,\ 0>t>t_2\\ (t_{h2}^9,\rho_{h2}^9)=(t,\rho)\ \Big|\ \dfrac{\partial g_{h2}}{\partial t}=0,\ \dfrac{\partial g_{h2}}{\partial \rho}=0,\\ \qquad\qquad\qquad\qquad 0>t>t_2,\ 0>\rho>-\mu\end{cases}$$

with $t_2 > t_1^*$

It is easy to find out:

$$\rho_{h2}^5=\lambda.a_{\max}/(2\phi.b_{\max})$$

$$\rho_{h2}^6=(\lambda.a_{\max}-2v_1^*.b_{\max})/(2\phi.b_{\max})$$

$$t_{h2}^7=c_1$$

$$t_{h2}^8=\frac{-\hat{a}}{2\sqrt{\hat{b}.f_2}}.\ln\left(\frac{\Delta a.\sqrt{\hat{b}.f_2}-\Delta b.\hat{a}.\sqrt{\dfrac{f_2}{\hat{b}}}+\mu.\phi.\hat{a}.b_{\max}}{\Delta a.\sqrt{\hat{b}.f_2}-\Delta b.\hat{a}.\sqrt{\dfrac{f_2}{\hat{b}}}-\mu.\phi.\hat{a}.b_{\max}}\right)-c_1$$

We can find the solutions for t_{h2}^9 and ρ_{h2}^9 in closed-form expressions, but they are too long to be presented here. Readers can try to find these expressions.

So, $\max(g_{h2})=\max\left\{g_{h2}(t_{h2}^i,\rho_{h2}^i)\right\},\ i=1,2...9$ (156)

Thus, the positive thrust margin *pTM* could be determined by Eqs. (147) and (152), or Eqs. (155) and (156).

5.2.2 Negative thrust margin *nTM*:

The formula of *nTM* can be achieved as below.

From Eq. (109), we have another inequality as follows:

$$\text{sat}(s/\phi) \le 1 \tag{157}$$

Multiplying both sides by -1, we have:

$$-\text{sat}(s/\phi) \ge -1$$

Then, multiplying both sides by K, we obtain:

$$-K.\text{sat}(s/\phi) \ge -K$$

Next, adding both sides by $\hat{u}$ yields:

$$\hat{u} - K.\text{sat}(s/\phi) \ge \hat{u} - K$$

Due to $u = \hat{u} - K.\text{sat}(s/\phi)$, the above inequality becomes:

$$u \ge \hat{u} - K \tag{158}$$

Substituting the expressions of $\hat{u}$ and K given in Eqs. (100) and (130) into the inequality (158):

$$\begin{aligned} u \ge\ & \hat{b}.\dot{z}\,|\dot{z}| + \hat{N} + \hat{a}.\ddot{z}_d - \lambda.\hat{a}.(\dot{z} - \dot{z}_d) \\ & -\Delta b.\dot{z}^2 - \Delta a.\left|\ddot{z}_d - \lambda(\dot{z} - \dot{z}_d)\right| - \Delta N - D - \eta.a_{\max} \end{aligned}$$

Due to $\dot{z}\,|\dot{z}| \le \dot{z}^2$, the following inequality can cover the above:

$$\begin{aligned} u \ge\ & \hat{b}.\dot{z}^2 - \Delta b.\dot{z}^2 + \hat{a}.\ddot{z}_d - \lambda.\hat{a}.(\dot{z} - \dot{z}_d) \\ & -\Delta a.\left|\ddot{z}_d - \lambda(\dot{z} - \dot{z}_d)\right| + \hat{N} - \Delta N - D - \eta.a_{\max} \end{aligned}$$

Due to $\hat{b} - \Delta b = b_{\min}$ and $\hat{N} - \Delta N = N_{\min}$, we have:

$$\begin{aligned} u \ge\ & b_{\min}.\dot{z}^2 + \hat{a}.\ddot{z}_d - \lambda.\hat{a}.(\dot{z} - \dot{z}_d) \\ & -\Delta a.\left|\ddot{z}_d - \lambda(\dot{z} - \dot{z}_d)\right| + N_{\min} - D - \eta.a_{\max} \end{aligned} \tag{159}$$

It is easy to realize that the control force can only get the minimum value in the deceleration period. So, we only need to consider the inequality (159) with the trajectories $\ddot{z}_d$, $\dot{z}_d$ designed for segments III. As a result, $\ddot{z}_d$ is negative. Due to $\lambda >$ 0, it is easy to realize that the right hand side of the inequality (159) gets smaller when the velocity error $(\dot{z}-\dot{z}_d)$ is non-negative. Therefore, we could only consider the below constraints:

$$u \geq b_{\min}.\dot{z}^2 + \hat{a}.\ddot{z}_d - \lambda.\hat{a}.(\dot{z}-\dot{z}_d) - \Delta a.\left|\ddot{z}_d - \lambda(\dot{z}-\dot{z}_d)\right| + N_{\min} - D - \eta.a_{\max} \quad (159)$$

with $\ddot{z}_d = \ddot{z}_{d3} < 0, \quad \dot{z}_d = \dot{z}_{d3} \geq 0, \quad (\dot{z}-\dot{z}_d) \geq 0, \quad \lambda > 0$ (160)

From the constraints (160), we deduce $\ddot{z}_d - \lambda(\dot{z}-\dot{z}_d) < 0$. So, $\left|\ddot{z}_d - \lambda(\dot{z}-\dot{z}_d)\right| = -\ddot{z}_d + \lambda(\dot{z}-\dot{z}_d)$. The inequality (159) becomes:

$$u \geq b_{\min}.\dot{z}^2 + (\hat{a}+\Delta a).\ddot{z}_d - \lambda.(\hat{a}+\Delta a).(\dot{z}-\dot{z}_d) + N_{\min} - D - \eta.a_{\max}$$

or, $u \geq b_{\min}.\dot{z}^2 + a_{\max}.\ddot{z}_d - \lambda.a_{\max}.(\dot{z}-\dot{z}_d) + N_{\min} - D - \eta.a_{\max}$ (161)

(due to $\hat{a}+\Delta a = a_{\max}$)

The term $\dot{z}^2$ is equivalent to $\left[(\dot{z}-\dot{z}_d)+\dot{z}_d\right]^2$. So, the inequality (161) can be rewritten as follows:

$$u \geq b_{\min}.\left[(\dot{z}-\dot{z}_d)+\dot{z}_d\right]^2 + a_{\max}.\ddot{z}_d - \lambda.a_{\max}.(\dot{z}-\dot{z}_d) + N_{\min} - D - \eta.a_{\max}$$

or, $u \geq a_{\max}.\ddot{z}_d + b_{\min}.\dot{z}_d^2 + N_{\min} + b_{\min}.(\dot{z}-\dot{z}_d)^2 - (\lambda.a_{\max} - 2b_{\min}.\dot{z}_d).(\dot{z}-\dot{z}_d) - D - \eta.a_{\max}$ (162)

From Eqs. (124) and (160), we have:

$$u_1 = \hat{a}.\ddot{z}_d + \hat{b}.\dot{z}_d^2 + \hat{N} \quad (163)$$

Then, from Eqs. (162-163), we deduce:

$$u \geq \Delta a.\ddot{z}_d - \Delta b.\dot{z}_d{}^2 + b_{\min}.(\dot{z} - \dot{z}_d)^2 - (\lambda.a_{\max} - 2b_{\min}.\dot{z}_d).(\dot{z} - \dot{z}_d) + u_1 - \Delta N - D - \eta.a_{\max} \quad (164)$$

Similar to the previous section, we substitute $(\dot{z} - \dot{z}_d) = \rho.\phi$ into the above inequality:

$$u \geq \Delta a.\ddot{z}_d - \Delta b.\dot{z}_d{}^2 + b_{\min}.\phi^2.\rho^2 - (\lambda.a_{\max} - 2b_{\min}.\dot{z}_d).\phi.\rho + u_1 - \Delta N - D - \eta.a_{\max} \quad (165)$$

with $0 \leq \rho \leq \mu$, due to $(\dot{z} - \dot{z}_d) \geq 0$ and $|\rho| \leq \mu$ from the constraints (142) and (160)

Set $g_l = \Delta a.\ddot{z}_d - \Delta b.\dot{z}_d{}^2 + b_{\min}.\phi^2.\rho^2 - (\lambda.a_{\max} - 2b_{\min}.\dot{z}_d).\phi.\rho$ (166)

From Eqs. (165) and (166), we should choose:

$$u_l = \min(g_l) + u_1 - \Delta N - D - \eta.a_{\max} \quad (167)$$

where $\min(g_l)$ is the minimum value of the function g_l.

So, we get the formula of *nTM* as follows:

$$nTM = u_l - u_1 = \min(g_l) - \Delta N - D - \eta.a_{\max} \quad (168)$$

The function g_l or $g_l(t,\rho)$, which is a function of two variables t and ρ, can get the minimum value at one of the following points:

$$(t,\rho)=\begin{cases}(t_l^1,\rho_l^1)=(t_2,0);\ (t_l^2,\rho_l^2)=(t_3,0)\\ (t_l^3,\rho_l^3)=(t_2,\mu);\ (t_l^4,\rho_l^4)=(t_3,\mu)\\ (t_l^5,\rho_l^5)=(t_2,\rho)\ \Big|\ \dfrac{dg_l(t_2,\rho)}{d\rho}=0,\ 0<\rho<\mu\\ (t_l^6,\rho_l^6)=(t_3,\rho)\ \Big|\ \dfrac{dg_l(t_3,\rho)}{d\rho}=0,\ 0<\rho<\mu\\ (t_l^7,\rho_l^7)=(t,0)\ \Big|\ \dfrac{dg_l(t,0)}{dt}=0,\ t_2<t<t_3\\ (t_l^8,\rho_l^8)=(t,\mu)\ \Big|\ \dfrac{dg_l(t,\mu)}{dt}=0,\ t_2<t<t_3\\ (t_l^9,\rho_l^9)=(t,\rho)\ \Big|\ \dfrac{\partial g_l}{\partial t}=0,\ \dfrac{\partial g_l}{\partial \rho}=0,\\ \qquad\qquad\qquad\qquad t_2<t<t_3,\ 0<\rho<\mu\end{cases}$$

with $t_2 > t_1^*,\ v_2 = v_m,\ t_3 = t_f = -c_4$

It is easy to find out:

$$\rho_l^5 = (\lambda.a_{\max} - 2v_1^*.b_{\min}) / (2\phi.b_{\min})$$

$$\rho_l^6 = \lambda.a_{\max} / (2\phi.b_{\min})$$

$$t_l^7 = t_3 = t_f = -c_4 \text{ (rejected)}$$

$$t_l^8 = \frac{-\hat{a}}{\sqrt{-\hat{b}.f_1}}.\arctan\left(\frac{\mu.\phi.b_{\min}.\sqrt{-\hat{b}/f_1}}{\Delta a.\hat{b}+\Delta b.\hat{a}}\right) - c_4$$

$$t_l^9 = \frac{-\hat{a}}{\sqrt{-\hat{b}.f_1}}.\arctan\left(\frac{\lambda.a_{\max}}{2.\sqrt{\frac{-f_1}{\hat{b}}}.(\Delta a.\hat{b}+\Delta b.\hat{a}+b_{\min})}\right) - c_4$$

$$\rho_l^9 = -\dot{z}_{d3}(t_l^9)/\phi + \lambda.a_{\max} / (2\phi.b_{\min})$$

So, $\min(g_l) = \min\left\{g_l(t_l^i,\rho_l^i)\right\},\ i = 1,2...9$ (169)

Thus, the negative thrust margin *nTM* could be determined by Eqs. (168) and (169).

5.2.3 μ-determination

As mentioned in Section 5.2.1, when the scalar quantity s is bounded

$$|s| \le \phi \tag{139}$$

the velocity error is also bounded. Obviously, the position error is too. Their bounds can be found in *Slotine* (*1983*) or *Slotine and Li* (*1991*).

We have the expression of s as given in Eq. (94):

$$s = (\dot{z} - \dot{z}_d) + \lambda(z - z_d) \tag{94}$$

Set $\tilde{z} = (z - z_d)$, position error (170)

So, $\dot{\tilde{z}} = \dfrac{d\tilde{z}}{dt} = (\dot{z} - \dot{z}_d)$, velocity error (171)

The expression of s can be rewritten as follows:

$$s = \dot{\tilde{z}} + \lambda.\tilde{z} \tag{172}$$

Due to $\tilde{z}(0) = 0$, taking the Laplace transform $\mathcal{L}$ of both sides of the above equation yields:

$$S = (p + \lambda).\tilde{Z} \tag{173}$$

where, p is the Laplace variable

$$S = S(p) = \mathcal{L}(s)$$

$$\tilde{Z} = \tilde{Z}(p) = \mathcal{L}(\tilde{z})$$

From Eq. (173), we have:

$$\tilde{Z} = \frac{1}{(p + \lambda)}.S \tag{174}$$

Next, taking the inverse Laplace transform of both sides of Eq. (174):

$$\tilde{z} = \mathcal{L}^{-1}\left\{\frac{1}{(p+\lambda)}\right\} * s \tag{175}$$

where, $\mathcal{L}^{-1}\{.\}$ is the inverse Laplace transform

the notation * denotes the convolution product

We have $$\mathcal{L}^{-1}\left\{\frac{1}{(p+\lambda)}\right\} = e^{-\lambda t} \tag{176}$$

So, according to the definition of convolution, Eq. (175) becomes:

$$\tilde{z} = \int_0^t e^{-\lambda.\tau}.s(t-\tau)d\tau \tag{177}$$

Due to $|s| \le \phi$, we deduces $|s(t-\tau)| \le \phi$. So, we have:

$$|\tilde{z}| \le \phi.\int_0^t e^{-\lambda.\tau}d\tau \tag{178}$$

Calculating the value of the integral at the right hand side of the above inequality, we obtain the bound of the position error as follows:

$$|\tilde{z}| \le \frac{\phi}{\lambda}.[1-e^{-\lambda t}] \le \frac{\phi}{\lambda} \tag{179}$$

(due to $e^{-\lambda t} \le 1$, with $t \ge 0$)

Now, let us find the bound of the velocity error. From Eq. (172), we have:

$$\dot{\tilde{z}} = s - \lambda.\tilde{z} \tag{180}$$

Due to $|s| \le \phi$ and $|\tilde{z}| \le \phi/\lambda$, we deduce the bound of the velocity error as follows:

$$|\dot{\tilde{z}}| \le \phi + \lambda.\frac{\phi}{\lambda} = 2\phi \tag{181}$$

So, if we set $\dot{\tilde{z}} = (\dot{z} - \dot{z}_d) = \rho.\phi$ and assume that $|\rho| \leq \mu$ as given in Eqs. (141-142), we easily deduce:

$$\mu = 2 \tag{182}$$

In fact, the much smaller than μ the bound of the velocity error can be if the shorter the response time of the actuator is. For this instance, we have:

$$|\rho| \leq \mu_r \ll \mu = 2$$

where μ_r is the real bound of the velocity error

A smaller value of μ_r makes the values of thrust margins smaller. This leads to a smaller thruster capacity required, which helps us save money. The value of μ_r should be determined by experiments.

5.3 Thruster capacity

The engineers need to know the required thrust range $[u_l \; u_h]$ to choose the thruster capacity for the thruster(s). This issue was mentioned in Section 5.2. The formulas calculating u_l and u_h are given in Eqs. (146) or (154) and (167). However, once the values of the thrust margins are available, u_l and u_h can be determined by the following simple formulas:

$$u_h = u_2 + pTM \tag{183}$$

$$u_l = u_1 + nTM \tag{184}$$

Thus, we should choose thruster(s) so that its thruster capacity covers the range $[u_l \; u_h]$.

Chapter 6

Simulation Results

In this chapter, the performance of the trajectory-tracking controller will be simulated by Matlab/Simulink.

6.1 Model parameters

In simulation, the estimated parameters of the mathematical model of the ROV Seamor are used. Their values, according to *Chen et al.* (*2007*), are listed in Table 6.1.

Table 6.1 The estimated parameters of the ROV Seamor

m (kg)	$Z_{\dot{w}}$ (kg/m)	$Z_{w\|w\|}$ (kg/m)
20.4	-68.576	-51.724

So, we have:

$$\hat{a} = m - Z_{\dot{w}} = 20.4 + 68.576 \simeq 89\,\text{kg} \qquad \hat{b} = -Z_{w|w|} \simeq 52\,\text{kg/m}$$

We assume that the parameters a and b have 20% uncertainty, the net buoyancy is fixed at 6N (no uncertainty), and the disturbance d is not larger than 5 N in absolute value. Table 6.2 and Table 6.3 show the estimated values and the bounds of the model parameters used in our simulations, respectively.

Table 6.2 The estimated values of the model parameters

$\hat{a}$ (kg)	$\hat{b}$ (kg/m)	$\hat{N}$ (N)	$\hat{d}$ (N)
89	52	6	0

Table 6.3 The uncertainty bounds

Δa (kg)	Δb (kg/m)	ΔN (N)	D (N)
17.8	10.4	0	5

6.2 Controller parameters

The parameters of the controller are given in Table 6.4.

Table 6.4 Controller parameters

λ (s^{-1})	ϕ ($m.s^{-1}$)	η ($m.s^{-2}$)	ξ
5	0.1	0.001	0.996

6.3 Thruster characteristics

The dynamics of the thruster(s) is ignored. Thruster(s) is assumed to have an instantaneous response to the controller's commands of force. The designed constant thrust forces are listed in Table 6.5.

Table 6.5 Designed thrust forces

u_1 (N)	u_2 (N)	u'_1 (N)	u'_2 (N)
-45	58	0	46

6.4 Milestones and landmarks

The milestones and landmarks which are used in designing the optimal trajectories are calculated from the designed thrust forces and the estimated parameters of the UV model. Their values are given in Table 6.6 for TOTs design and in Table 6.7 for ESTs design.

Table 6.6 Milestones and landmarks used for TOTs design

v_m (m/s)	t_1^* (s)	v_1^* (m/s)	z_1^* (m)	Δz_3^* (m)	z_e^* (m)
1.0	5.32	0.996	4.13	0.6	4.74

Table 6.7 Milestones and landmarks used for ESTs design

v_m (m/s)	t_1^* (s)	v_1^* (m/s)	z_1^* (m)	Δz_3^* (m)	z_e^* (m)
0.877	6.06	0.874	4.13	1.74	5.88

6.5 Simulation and analysis

6.5.1 Simulation 1

In the first simulation, TOTs of Plan I are used. The ending depth is 8m, which is greater than z_e^* = 4.74m (see Table 6.6). The controller is applied to the UUV model without uncertainties to check the clinging ability of the control force to the designed thrust force. The simulation results for this case are shown in Fig. 6.1.

For this case, the ending time is 9.95s. Segment I lasts from 0 to 5.32s, segment II from 5.32 to 8.58s, segment III from 8.58 to 9.95s, and segment IV from 9.95s onwards.

In Fig. 6.1a, the control force is almost equal to the designed force except for the short periods of time at the beginning of each segment. Force deviation in these periods does not exceed 2 N because these are transitional periods of the control system. At rest status (segment IV), the controller maintains a force of 6N to balance the net buoyancy. This helps the vehicle keep its depth constant.

Fig. 6.1b-d show that the acceleration, velocity, and depth of the vehicle track the designed trajectories very well. Maximum absolute errors of the acceleration, velocity, depth are 26.4 mm/s^2, 4mm/s, and 2.5mm, respectively.

As shown in Fig. 6.1b, the acceleration is about 0.584m/s^2 at the beginning. It decreases to zero during segment I, and remains at zero in segment II. At the initial point of segment III, it decreases to the peak negative value of -1.16m/s^2. And then, it increases to -0.573 m/s^2 during segment III. At the initial point of segment IV, it decreases to zero, and stays at this value afterwards.

Fig. 6.1c shows that the velocity increases from 0 to 1m/s during segment I, and stays at this value in segment II. And then, it decreases from 1m/s to zero in segment III, and stays at this value of zero afterwards.

The controller helps the vehicle move smoothly to the ending depth as shown in Fig. 6.1d.

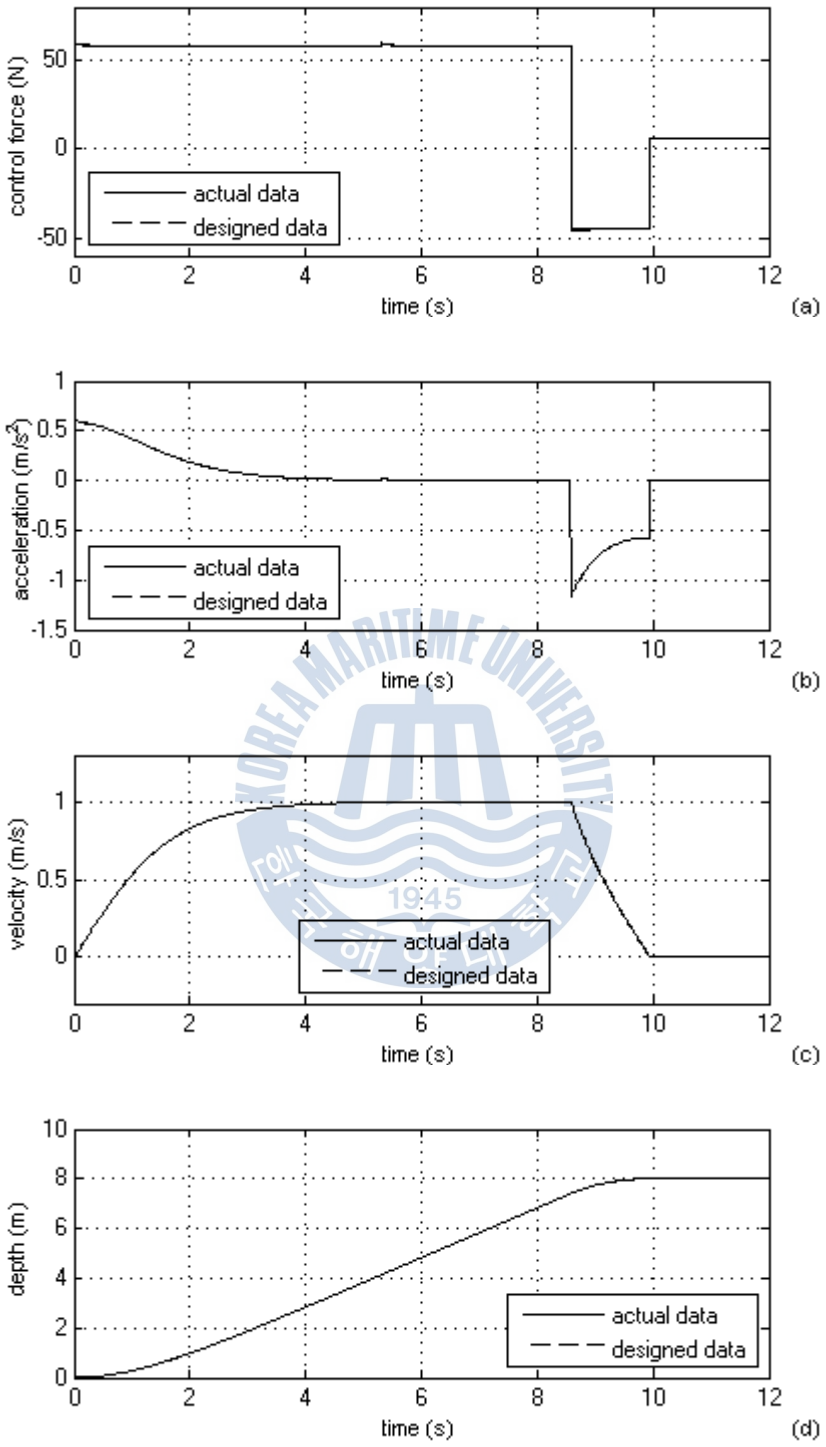

Fig. 6.1 Simulation results without uncertainties for TOTs of Plan I

6.5.2 Simulation 2

In the second simulation, TOTs of Plan II are used. The ending depth is just 2m, which is less than z_e^* = 4.74m (plan II). The UUV model also has no uncertainties. The simulation results are shown in Fig. 6.2.

For this case, the ending time is 3.87s. Segment I lasts from 0 to 2.58s, segment II from 2.58 to 3.87s, and segment III from 3.87s onwards.

Fig. 6.2b shows that the vehicle acceleration is 0.584m/s^2 at the beginning, and that it decreases to 0.105m/s^2 during segment I. At the initial point of segment II, it decreases to the peak negative value of -1.06m/s^2. And then, it increases to -0.573 m/s^2 during segment II. At the initial point of segment III, it decreases to zero, and stays at this value afterwards.

Fig. 6.2c shows that the velocity increases from 0 to 0.91m/s during segment I, and then, decreases to zero in segment II, and maintains this value of zero in segment III.

The control force and the depth track the designed trajectories very well as shown in Fig. 6.2a&d.

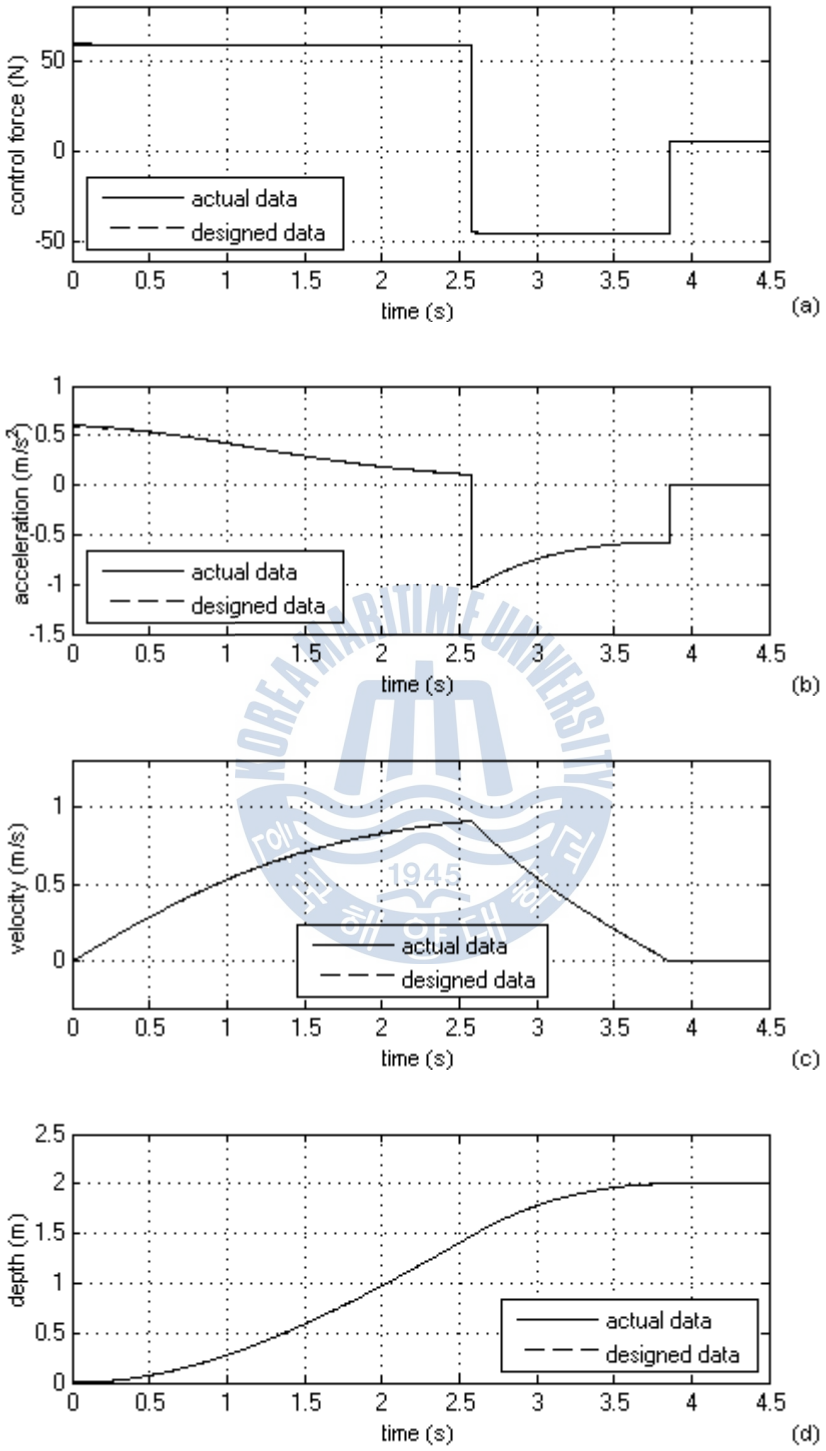

Fig. 6.2 Simulation results without uncertainties for TOTs of Plan II

6.5.3 Simulation 3

In this simulation, TOTs of Plan I are used, the ending depth is 8m. But the controller is applied to the UUV model with uncertainties as shown below.

$$a = \hat{a} + \Delta a.\sin(2 \mid \dot{z} \mid .t)$$

$$b = \hat{b} + \Delta b.\sin(2 \mid \dot{z} \mid .t)$$

$$N = \hat{N}$$

$$d = D.\sin(2t + \pi)$$

The simulation results for this model with 20% uncertainty of a and b are shown in Fig. 6.3.

The existence of the uncertainties forces the controller to give out the commands of force whose values could be greater or less than the designed force. Because the uncertainties are sinusoidal, the control force is also sinusoidal to mitigate their effects as shown in Fig. 6.3a. So, the acceleration and velocity oscillate around the designed trajectories as shown in Fig. 6.3b&c.

As shown in Fig. 6.3a, the maximum and minimum control forces were 73.06 and -70.4 N, respectively. The maximum absolute errors of acceleration, velocity, depth are 444mm/s^2, 28.2mm/s, and 13.7mm, respectively. The depth error at steady state (segment IV) does not exceed 5.4mm. This error could be smaller if the parameter λ was a higher value.

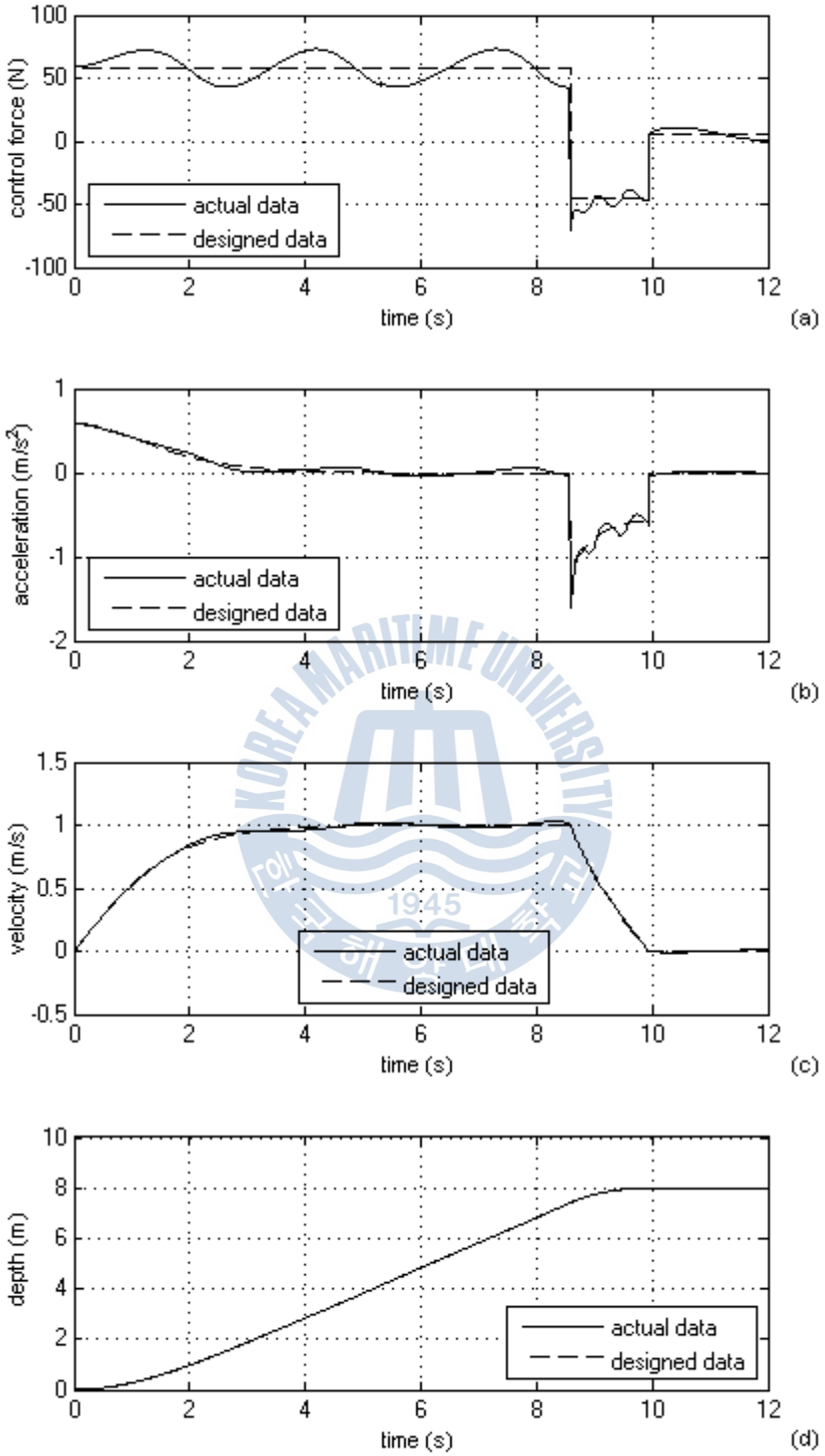

Fig. 6.3 Simulation results with 20% uncertainty for TOTs of Plan I

Through the first and second simulations, the time optimality of the designed trajectories was validated. In both cases (plan I & II), the control system always uses the control forces which are almost equal to the designed forces. If these designed forces are equal to the maximum forward or reverse thrust force of the thruster(s), the travel time of the vehicle to the destination could be considered to be the minimum. However, they should be chosen to be less than the maximum thrust forces of the thruster(s) so that the thrust margins are large enough for the thruster(s) can meet the potential maximum commands of the control force, even with uncertainties. This helps to ensure that the vehicle can track the designed trajectory as well as expected. In the latter case, the travel time might not be the minimum, but a predictable and reasonable one. Moreover, the overshoot of the depth could be controlled very well. For these reasons, the designed trajectories are named the time-optimal trajectories. They are suitable for driving the vehicle over a relatively short distance with requirements of exact time and position. For long distance, these requirements no longer become important, and the vehicle can use the maximum thrust forces to reach the destination depth quickly.

Our controller is designed based on the assumption that the parameters a and b have 20% uncertainty. If the uncertainty of these parameters is not greater than 20%, the performance of the controller is good as shown in Fig. 6.3. On the contrary, the performance is bad, even failure in tracking.

In the next simulation, we assume that a and b have 50 or 100% uncertainty, and the thrust range of the thruster(s) is [-100 100] (N). The simulation results for this case are shown in Fig. 6.4.

In Fig. 6.4d, we see that the depth in case of 50% uncertainty can still track the designed depth although the depth error increases to 2.4cm, and the control force is required to 83.25 or -88.25N (Fig 6.4a). However, the depth in case of 100% uncertainty cannot track the designed depth. The reason is that the control force required exceeds the capacity of the thruster(s). As a result, the controller fails in tracking control.

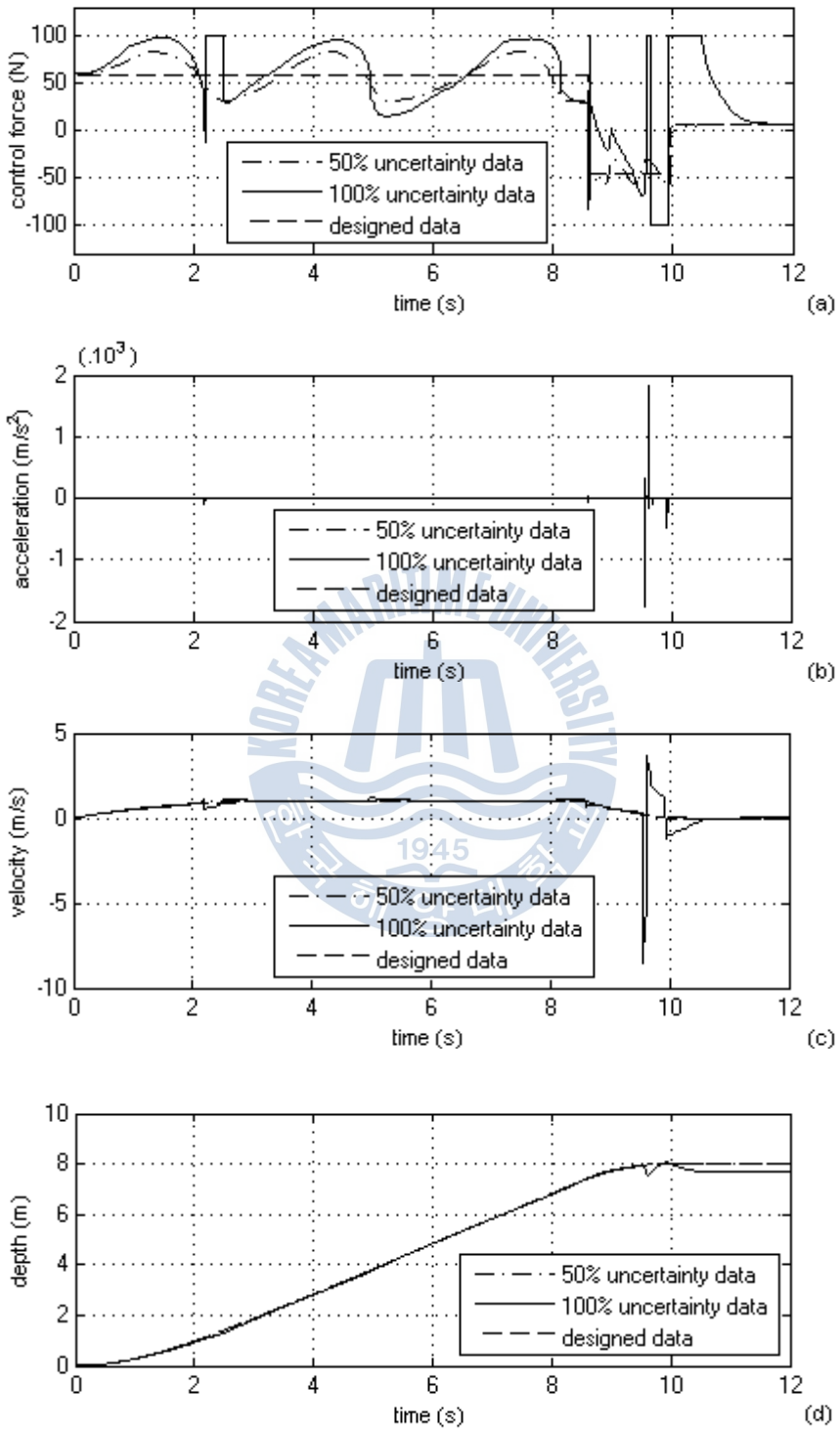

Fig. 6.4 Simulation results with 50 and 100% uncertainty for TOTs of Plan I

6.5.4 Simulation 4

In this simulation, ESTs of Plan I are used. The ending depth is 8m, which is greater than z_e^* = 5.88m (see Table 6.7). The UUV model has no uncertainties. The simulation results for this case are shown in Fig. 6.5.

For this case, the ending time is 14.54s. Segment I lasts from 0 to 6.02s, segment II from 6.02 to 8.48s, segment III from 8.48 to 14.54s, and segment IV from 14.54s onwards.

In Fig. 6.5a, the control force is almost equal to the designed force (46N for the constant velocity and acceleration periods, 0N for the deceleration period) except for the short periods of time at the beginning of each segment. Force deviation in these periods does not exceed 2 N because these are transitional periods of the control system. At rest status (segment IV), the controller maintains a force of 6N to balance the net buoyancy. This helps the vehicle keep its depth constant.

Fig. 6.5b-d show that the acceleration, velocity, and depth of the vehicle track the designed trajectories very well. Maximum absolute errors of the acceleration, velocity, depth are 24.4 mm/s^2, 3.5mm/s, and 1.4mm, respectively.

As shown in Fig. 6.5b, the acceleration is about 0.517m/s^2 at the beginning. It decreases to zero during segment I, and remains at zero in segment II. At the initial point of segment III, it decreases to the peak negative value of -0.517m/s^2. And then, it increases to -0.067 m/s^2 during segment III. At the initial point of segment IV, it decreases to zero, and stays at this value afterwards.

Fig. 6.6c shows that the velocity increases from 0 to 0.877m/s during segment I, and stays at this value in segment II. And then, it decreases from 0.877m/s to zero in segment III, and stays at this value of zero afterwards.

The controller helps the vehicle move smoothly to the ending depth as shown in Fig. 6.5d. Although the travel time is longer than the one of TOTs in the first simulation, the energy consumption is minimal.

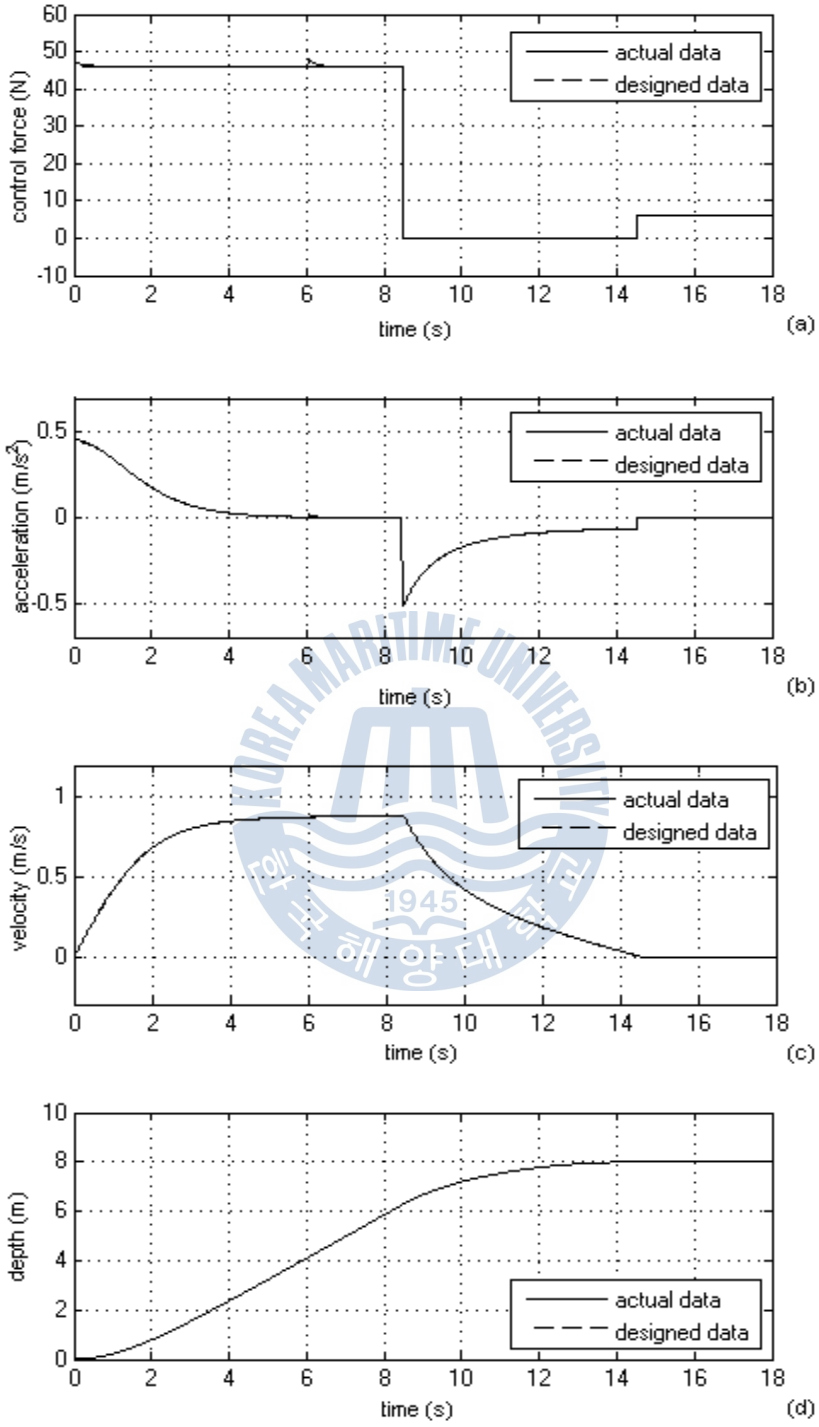

Fig. 6.5 Simulation results without uncertainties for ESTs of Plan I

Chapter 7

Conclusions

In this dissertation, the design of the optimal-trajectories including time-optimal trajectories and energy-saving ones used for the depth control of UUVs was presented. The time-optimal trajectories are designed based on the idea of always using the constant thrust forces whose values are chosen reasonably during the maneuver. For energy-saving trajectories, their designs stems from using thrust forces at which the efficiency of thruster(s) is maximum, and from an energy-efficient control strategy in which the accumulated kinetic energy of vehicle will be fully utilized in motion control, i.e., the thruster(s) is not used to brake the vehicle velocity during the maneuver. These trajectories are the explicit functions, which are the analytical solutions of the nonlinear second order differential equation representing the depth motion of the UUV. The analytical solutions offer more advantages than the numerical ones such as easy calculation, simple and unaltered form, convenient use, etc. Although the proposed solutions are assigned to the depth control, those can be applied to other direction motion control of UUVs, or to systems with similar structure and control objective. Furthermore, it is also not difficult to get the corresponding solutions in which the values of the beginning and ending velocities (v_0 and v_e) may be different from zero. If these trajectories are used along with a robust trajectory-tracking controller, time-optimal or energy-efficient maneuver can be achieved.

The dissertation proposed a trajectory-tracking controller using the siding mode method. It is shown that even with uncertainties, this controller can force the vehicle states to the designed optimal trajectories. Its robustness can be guaranteed if bounds of the uncertainties are known. The effectiveness of the combination of the above optimal trajectories and this trajectory-tracking controller was demonstrated via simulation results. If there are not the influences of the uncertainties, the control forces of the controller will be nearly equal to the

designed constant forces, on the contrary, they could be different. Therefore, the thruster(s) should be chosen so that it can meet the requirements of control force of the controller.

The dissertation also presented the calculation of the thrust range required by the trajectory-tracking controller. The limit values of the thrust range are references for engineers to decide thruster capacity for choosing the thruster(s).

References

Chen, H.H., Chang, H.H., Chou, C.H., Tseng, P.H., 2007. Identification of hydrodynamic parameters for a remotely operated vehicle using projective mapping method. Symposium on Underwater Technology and Workshop on Scientific Use of Submarine Cables and Related Technologies.

Chyba, M., Haberkorn, T., Smith, R.N., Choi, S.K., 2008a. Autonomous underwater vehicles: Development and implementation of time and energy efficient trajectories. Ship Technology Research. Vol. 55, no. 2, pp. 36-48.

Chyba, M., Haberkorn, T., Smith, R.N., Choi, S.K., 2008b. Design and implementation of time efficient trajectories for an underwater vehicle. IEEE Journal of Ocean Engineering. Vol. 35, no. 1, pp. 63-76.

Fossen T.I., 1994. Guidance and Control of Ocean Vehicles. John Wiley and Sons, New York.

Fraga, S.L., Sousa, J.B., Pereira, F.L., 2003. Trajectory generation for a remotely operated vehicle. IEE European Control Conference.

Prestero T., 2001. Verification of a six-degree of freedom simulation model for the REMUS autonomous underwater vehicle. M.S. Thesis. MIT, USA.

Slotine, J.J., 1983. Tracking control of nonlinear systems using sliding surfaces. PhD Dissertation. MIT, USA.

Slotine, J.J., Li, W., 1991. Applied Nonlinear Control. Prentice Hall.